sustainability

MDPI

Article

Unveiling the Coupling Coordination and Interaction Mechanism between the Local Heat Island Effect and Urban Resilience in China

Huihui Wang [1,2,3,*,†], Yunsong Yang [1,2,3,†], Suru Liu [1,4,†], Hanyu Xue [1,5], Tingting Xu [1,6], Wanlin He [1,4], Xiaoyong Gao [1,7] and Ruifeng Jiang [1,6]

1 Advanced Institute of Natural Sciences, Beijing Normal University, Zhuhai 519087, China; 202321180071@mail.bnu.edu.cn (Y.Y.); 202111069040@mail.bnu.edu.cn (S.L.); 202111069033@mail.bnu.edu.cn (H.X.); 202111079054@mail.bnu.edu.cn (T.X.); 202111069011@mail.bnu.edu.cn (W.H.); 201911039071@mail.bnu.edu.cn (X.G.); 202011059358@mail.bnu.edu.cn (R.J.)
2 School of Environment, Beijing Normal University, Beijing 100875, China
3 Key Laboratory of Coastal Water Environmental Management and Water Ecological Restoration of Guangdong Higher Education Institutes, Beijing Normal University, Zhuhai 519087, China
4 Zhixing College, Beijing Normal University, Zhuhai 519087, China
5 Research Institute of Urban Renewal, Zhuhai Institute of Urban Planning and Design, Zhuhai 519100, China
6 Huitong College, Beijing Normal University, Zhuhai 519087, China
7 Department of Geography, National University of Singapore, Singapore 117570, Singapore
* Correspondence: wanghui@bnu.edu.cn
† These authors contributed equally to this work.

Abstract: Climate change and urbanization have led to the increasing prominence of urban heat islands (UHIs) today, posing a huge challenge to cities. Urban resilience (UR) refers to the ability of a city or region to adapt to changes and risks. However, the influence between the heat island effect and regional urban resilience is not well understood. In this study, we proposed a methodological framework for unveiling the coupling coordination and interaction mechanism between UHIs and UR. This study first explored UHIs in the Guangdong-Hong Kong-Macao Greater Bay Area (GBA) and described the creation of a multidimensional index system that evaluates urban resilience across social, economic, ecological, and engineering dimensions. Furthermore, this study unveiled the coupling coordination effect of UHIs and UR through the coupling coordination degree model, and the influence mechanism between the drivers of UHIs and the change in UR was detected using a geographic probe. The results showed that the UHI region forms a ring-shaped belt around the entrance to the Pearl River Delta. The UHIs of the GBA show a significant trend of expansion and escalation over time. The UR of the GBA shows a spatial distribution pattern of high resilience among regional central cities and low resilience among peripheral cities, with significantly uneven development in sub-resilience dimensions. The UHIs and UR of the GBA showed a certain coupling and coordination effect, improving from barely synergistic to a primary coordination state. Among the drivers of UHIs, population density, precipitation, average nighttime light brightness, and ground-average CO_2 emissions have strong explanatory power for the spatial variation in UR. The interaction between two factors has a stronger influence on UR than individual factors. The purpose of this paper is to initially reveal the influence mechanism between UHIs and UR and to provide a theoretical basis for further exploring the path of sustainable urban development.

Keywords: urban heat islands; urban resilience; coupling coordination degree; interaction mechanism; Guangdong-Hong Kong-Macao Bay Area

check for updates

Citation: Wang, H.; Yang, Y.; Liu, S.; Xue, H.; Xu, T.; He, W.; Gao, X.; Jiang, R. Unveiling the Coupling Coordination and Interaction Mechanism between the Local Heat Island Effect and Urban Resilience in China. *Sustainability* **2024**, *16*, 2306. https://doi.org/10.3390/su16062306

Academic Editor: Salvador García-Ayllón Veintimilla

Received: 22 January 2024
Revised: 29 February 2024
Accepted: 6 March 2024
Published: 11 March 2024

Copyright: © 2024 by the authors. Licensee MDPI, Basel, Switzerland. This article is an open access article distributed under the terms and conditions of the Creative Commons Attribution (CC BY) license (https://creativecommons.org/licenses/by/4.0/).

1. Introduction

With the rapid development of the global economy, an increasing number of people are concentrated in urban areas [1]. China is one of the most rapidly urbanizing developing

countries, and due to the rapid growth of the urban population and continuous expansion in urban scale, the nature of the urban substratum and canopy structure has changed significantly as a result, while anthropogenic heat release from cities has been increasing, causing increasingly serious urban environmental problems, including air pollution and urban heat islands (UHIs) [2]. The increasing frequency of disasters and extreme weather events due to global climate change [3,4] has devastating effects on human society, infrastructure, and ecology [5–8], posing an incalculable risk potential for cities.

Urban heat islands (UHIs) are a phenomenon by which the temperature of a city is higher than that of the surrounding suburban environment [9], and it is an important factor affecting the quality of the urban environment. UHIs lead to increased urban energy consumption, increased greenhouse gas emissions, and significant impacts on local meteorology, air quality, vegetation growth, and human health [10–13]. The occurrence of UHIs is closely related to climate change and urbanization. Scholars' studies on UHI drivers have found that surface vegetation cover, wind speed, and precipitation have significant effects on urban temperature changes [14–17]. With rapid urbanization, socioeconomic factors, including carbon dioxide (CO_2) emissions, population density, gross domestic product, nighttime lighting, and the degree of urban development, may play an important role in exacerbating UHIs through anthropogenic heat emissions [18–21]. Landscape urbanization, including urban expansion and densification, further leads to widespread UHI phenomena by altering the land capacity to evaporate water and the efficiency to convect heat into the lower atmosphere [22–25]. UHIs exacerbate various problems and risks in the process of urbanization, while urbanization has also made the emergence of UHIs more frequent. There is a complex interactive coupling relationship between UHIs and urbanization, which brings enormous uncertainty to urban development planning and management. Based on the current trends of climate change, urban population growth, and continued urbanization, Chinese cities also need to address the environmental pressures and challenges associated with rapid urban development [26].

Traditional urban planning and management tend to respond to external threats with a rigid defense strategy, ignoring the inherent organizational, coordination, and adaptive capabilities of the urban system [27]. It requires people to have a high level of risk control ability, as the fragility of technology and social systems cannot be fully predicted [28], which may lead to the accumulation of risks, especially in the context of complex and unpredictable factors, such as climate change. It leads to greater unexpected losses than before implementing defensive policies once the system is hit beyond the maximum threshold of urban planning [29,30]. Therefore, it is necessary to address such challenges from a new perspective.

The concept of "resilience" was first introduced in ecology by Holling [31], who proposed that resilience is the ability of a system to anticipate and resolve external shocks while maintaining its primary function in the event of a crisis. Moreover, this concept has been continuously enriched [32,33], and related theories have also been gradually applied to several disciplines, including economics, human development, and urban planning [34–38]. Urban resilience (UR), a new way of thinking about urban risk management, focuses on the organization and function of the urban system itself to enhance the ability to coordinate and adapt to uncertainty and to protect the sustainable development of cities under the continuous impact of climate change. Some researchers have absorbed the perspective of "resilience" in their research on UHIs but still remain focused on predicting UHIs [39–41] or studying the influencing factors of UHIs. They consider "urban resilience" more as a planning and management goal or policy background rather than the attribute of urban systems maintaining normal functional states under the uncertainty impact of UHIs. These studies did not focus on the resilience states of various subsystems (which possess certain important functions) under the impact of UHIs and, therefore, did not further explore the interaction mechanism between UHIs and UR. The complexity of the urban system cannot simply be reflected by a single function. For instance, after the economic system is affected by a UHI, it may cause a chain reaction, such as unemployment, which aggravates social instability.

Extreme high-temperature events may increase the risk of high temperature-related incidence rates and mortality [42–45] and also endanger the health of the population and the stability of the social structure. Moreover, abnormal high-temperature climates may cause urban water environments and ecological deterioration [22,25,46,47]. In addition, it may also affect energy consumption [24,47], impacting the availability of resources for residents. From these aspects, UHIs will increase the cost of recovering urban system functions from damage. However, we should also recognize that urban systems rebuild from damaged states, relying on flexible social structure, active human activities, material production, and energy consumption; that is, the development of resilience comes at the cost of a certain degree of heat production. Therefore, in order to comprehensively consider the interaction between UR and UHI phenomena, we attempt to construct a multidimensional resilience indicator system to include additional important urban subsystems in social, ecological, and engineering functions and use the UR results to study the interaction relationship with UHIs. Previous studies have focused on the bidirectional causal feedback relationship between UHI phenomena and economic systems but have not comprehensively considered the involvement of other functional subsystems in complex interactions [48]. There have been many studies on UHIs based on remote sensing inversion [49,50], and the studies on UR evaluation and influencing factors have gradually become a research hotspot [51–54]. In addition to the abnormal high-temperature characteristics caused by the UHI phenomenon, we have considered some conditions that may drive the occurrence of UHIs, namely the driving factors of UHIs. If the generation of UHIs is essentially driven by certain factors, are these factors also related to the state of UR? However, previous studies have not yet paid attention to possible connections between UR status and driving conditional factors of UHIs and have not provided a comprehensive analysis. In view of this, we applied the geographic probes to test whether the driving factors of UHIs control the spatial differentiation of UR, thereby further revealing the relationship between UHIs and UR in different potential processes.

China has experienced rapid urbanization since 1978, during which the Guangdong-Hong Kong-Macao Greater Bay Area (GBA) has undergone a dramatic urban expansion [55]. With the increase in population, energy consumption, and anthropogenic heat generation, urban systems will face risks brought by UHIs in terms of resilience in multiple functional subsystems, such as economy, society, ecology, and engineering. In this study, we proposed a methodological framework for unveiling the coupling coordination and interaction mechanism between UHIs and UR. First, UHIs were quantified and classified by introducing the heat island proportion index to analyze their spatial and temporal evolution during the period of 2000–2019. We expect to ensure that a heat island phenomenon occurs in the study area and understand to what extent it approaches the least ideal state of UHI. Then, a four-dimensional UR evaluation index system of "social–economic–ecological–engineering" was established by selecting relevant indicators, considering the resilience of each functional subsystem of the urban system as fully as possible, and the UR level was evaluated through the entropy weight TOPSIS evaluation model. The evaluation weights of each indicator are objectively derived from the information of the data itself, and the TOPSIS evaluation model calculates the UR level scores and provides a relative proximity ranking of approaching the ideal value of historical observation data. On this basis, the degree of synergistic changes and development between UHIs and UR in the study area was analyzed based on the coupling coordination degree model, and the interaction mechanism of the drivers of UHIs on the change in UR and urban subsystems was detected using geographic probes. By unveiling the coupling coordination and influence mechanism between UHIs and UR, this study changes the research perspective on UHIs from common remote sensing inversion and model prediction to how UHIs affect the functional maintenance and restoration of the urban system itself and provides a theoretical basis for further exploring how cities can cope with the pressure and challenges that UHIs caused, enhancing resilience and implementing a sustainable development path.

2. Materials and Methods

2.1. Study Area

The GBA contains Hong Kong, Macao and nine cities in the Pearl River Delta, Guangzhou, Shenzhen, Zhuhai, Foshan, Zhongshan, Dongguan, Zhaoqing, Jiangmen, and Huizhou (Figure 1), covering an area of approximately 55,900 km^2. The area is in the low-latitude zone, bordering the ocean and surrounding the mouth of the Pearl River, with a tropical and subtropical humid monsoon climate, so it is cloudy and rainy all year round, with long summers and short winters. The average annual temperature in the region is approximately 23 °C, and the average annual precipitation is over 1500 mm. The average altitude of the region is below 200 m, with more low hills and mountains, while the central and coastal areas are gentler. The social and economic development of the GBA is more prosperous, and the total population of the GBA exceeded 70 million in 2019, accounting for approximately 5% of the total population of the country, creating a GDP of approximately 12% of the national share, amounting to more than 10 trillion CNY.

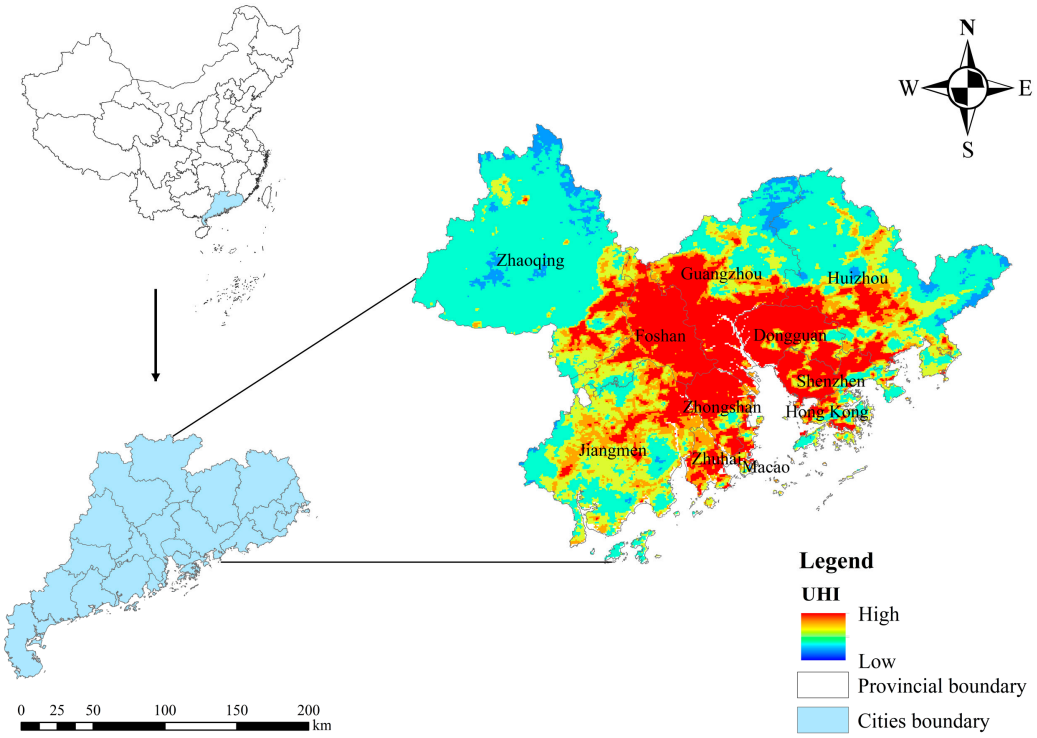


Figure 1. Study area of the GBA in China.

2.2. Methodology

2.2.1. Methodological Framework

Climate change has led to increased urban warming and extreme weather events, coupled with the effects of urban land expansion and population growth due to urbanization, resulting in the increasingly severe UHI phenomenon today, and UHIs pose a huge challenge to the fundamental attributes of urban systems in absorbing risks and recovering from shocks. In this study, we proposed a methodological framework for unveiling the coupling coordination and interaction mechanism between UHIs and UR to provide effective recommendations for the planning and management of UR and sustainable development under the oppression of UHIs (Figure 2). First, the study used MODIS data to obtain the surface temperature of the GBA. The UHIs were obtained based on the urban–rural temperature difference, and the urban heat island proportion index (UHPI) was calculated to quantitatively analyze the UHIs in the GBA. Subsequently, focusing on the resilience characteristics of the city itself in absorbing and adapting to risk shocks, from the four-dimensional perspectives of society, economy, ecology, and engineering, an UR evaluation

index system was established to measure the UR of the study area. Then, through the coupling coordination degree model, the closeness of common changes and the level of common development between the two systems of UHIs and UR in the study area were analyzed. Ultimately, a geographic probe was introduced to detect the influence mechanism of the drivers of UHIs on the change in UR. Based on the research on the spatiotemporal evolution trends, the coupling coordination degree, and impact mechanisms of UHIs and UR, this study proposed management suggestions for controlling the driving factors of UHIs under the risk scenario of UHIs in order to maintain urban system functionality and development resilience while reducing UHI risks.

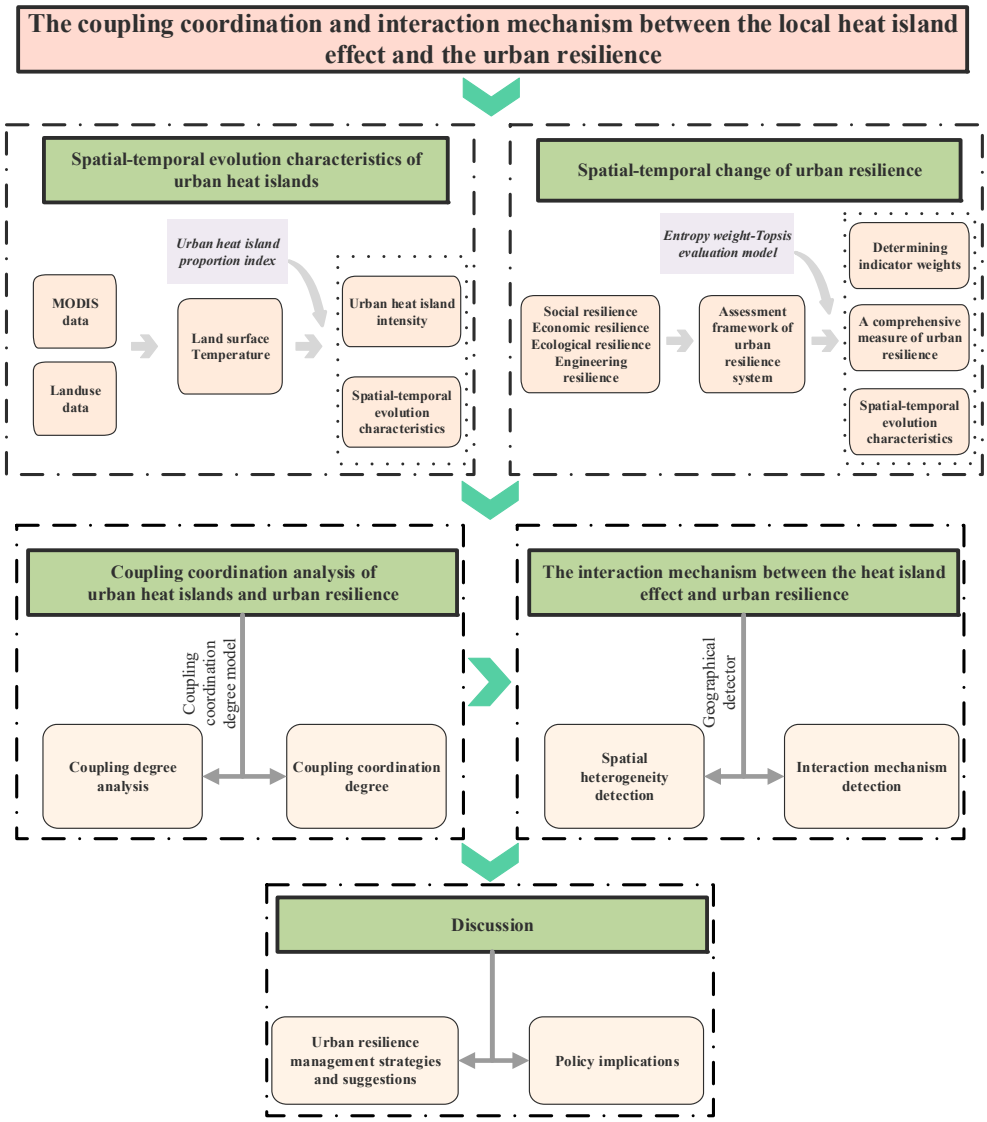


Figure 2. The framework of the study.

2.2.2. Measuring Urban Heat Islands

The process of preprocessing MODIS data and extracting UHIs is shown in Figure 3. First, the MOD11A2 data were reprojected, and the images of the study area were cropped using the vector boundaries of the study area. Then, the daytime and nighttime data were fused by extracting two band datasets, LST__Day__1 Km and LST__Night__1 km, respectively, in ENVI 5.3 and applying the band transport algorithm by inputting the formula (b1 + b2)/2 in the band calculator to average the daytime and the nighttime to obtain the 8d averaged data [56,57]. The land surface temperature was extracted to obtain

the land surface temperature distribution of the GBA. Land surface temperature (LST) is a quantitative indicator that directly responds to the thermal field. The MODIS surface temperature product was used to represent the thermal field distribution, and the DN value that represents the brightness temperature value in the MOD11A2 data needed to be converted to the real surface temperature, and the calculation formula is as follows:

$$LST = a * pixelv + b, \quad (1)$$

where LST is the true temperature value of the calculated pixel, pixelv is the greyscale value of the pixel, a is the scale factor, and b is the offset. Here, a = 0.02 and b = −273.15.

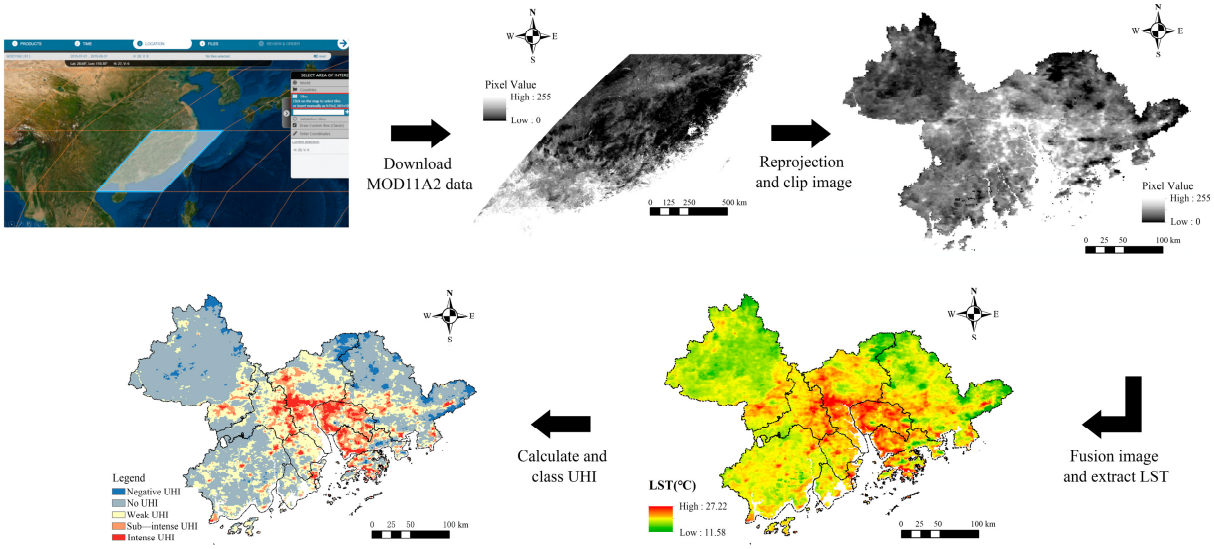


Figure 3. The process of preprocessing MODIS data and extracting UHIs.

UHIs are a phenomenon where the temperature or surface temperature of a city is higher than the temperature of the surrounding suburban areas, which is generally expressed as the difference in surface temperature between urban and suburban areas. In this study, the area 3 km away from the urban land (construction land) was taken as the suburban background; the surface temperature data on its corresponding image element were extracted, and the mean value , which is the average suburban background temperature of Guangdong, Hong Kong, and Macao, was calculated, and the formula is as follows:

$$UHI = LST - LSTs, \quad (2)$$

where UHI is the urban heat island intensity, and a value greater than 1 indicates the existence of the heat island effect; LST is the surface temperature; and LSTs is the average of the background surface temperature in the suburban areas. To reflect the spatial distribution characteristics of UHIs in Guangdong, Hong Kong, and Macao, the measured UHIs are divided into five classes from weak to strong, as shown in Table 1. The grade value can characterize the degree of development of the urban heat island. The larger the grade value, the stronger the effect of the urban heat island.

Table 1. Classification of UHI intensity.

Grade	UHI Intensity Range	UHI Rating
1	<−1	Negative UHI
2	−1~1	No UHI
3	1~2	Weak UHI
4	2~3	Sub-intense UHI
5	>3	Intense UHI

The UHPI was used to estimate the urban surface heat island intensity, which can quantitatively reflect the spatial and temporal differences in UHIs and is calculated as follows:

$$\mathrm{UHPI} = \sum_{i}^{\mathrm{n}} w_i p_i / (100 \times \mathrm{m}), \quad (3)$$

where UHPI is the urban heat island proportion index; m is the number of UHI intensity levels; i is the UHI intensity grades in urban areas that are higher than those in suburban areas; n is the number of UHI intensity grades in urban areas that are higher than those in suburban areas; w_i is the weight of different UHI intensity grades, taking the value of grade i as the weight; and p_i is the percentage of area occupied by grade i, and its value is between 0 and 100. The UHPI value is between 0 and 1, and the larger the value is, the closer to the least ideal state of the UHI and the more serious the UHI phenomenon is. Here, the UHI intensity is divided into five grades. It can be calculated that the UHI intensity in suburbs is highest at grade 2, while the UHI intensity in urban areas, which is partly higher than that in suburbs, is distributed among grades 3, 4, and 5 and is highest at level 5. Therefore, m = 5, i = 3, 4, 5, and n = 3.

The UHPI is calculated as the ratio of the area of the heat island in the spatial extent to the area of the region where it is located, and weights were assigned to characterize the degree of development of the heat island in the spatial unit so that this value can not only effectively compare the strength of the heat island in different spatial units but also compare the size of the intensity of the heat island in the same region in different periods. The stronger the heat island effect is, the more significant the impact on the UHPI is, and the weaker the heat island effect is, the smaller the impact on the UHPI is. Therefore, the use of the rank value as the weight in the calculation of the UHPI can accurately reflect the strength of UHIs in the region.

2.2.3. Indicator System Construction

In this paper, based on the four-dimensional perspective of social–economic–ecological–engineering and the actual development of the GBA during the period of 2000–2019, four to six indicators were selected for each dimension [58], forming a resilience evaluation system containing 21 evaluation indicators (Table 2) to develop UR measurements for cities in the GBA.

Social resilience (SR) embodies the urban social system's capacity to navigate risks and guides the primary trajectory of urban crisis management. Hence, we selected five key indicators: population density, the ratio of college students per 1000 residents, the proportion of tertiary industry workers, the quantity of patent applications, and the year-end urban registered unemployment rate. These indicators offer insights into population dynamics, employment trends, and innovation prowess. The urban registered unemployment rate serves as a barometer of employment stability, reflecting the city's social equilibrium. Strong social support structures and effective governmental interventions are pivotal in mitigating challenges stemming from high unemployment rates. The number of college students per thousand residents and the volume of patent applications gauge the city's educational and research innovation landscape, indicative of its resilience to emergent risks [53,59]. Social management personnel, predominantly sourced from the tertiary sector, play a critical role in upholding urban functionality during crisis scenarios [60,61].

Economic resilience (ENR) is frequently assessed using key economic proxies, such as GDP. In this study, we selected five indicators from the China City Statistical Yearbook under the category of "Economic Development" to holistically evaluate economic resilience. GDP per capita serves as a macroeconomic indicator, representing productivity and living standards. The proportion of the tertiary industry in GDP was chosen to depict the industrial structure, which also signifies industrial adaptation towards emission reduction. Per capita disposable income of urban residents reflects the financial resources available to urban dwellers. Total import and export value provides insights into the overall scale and developmental stage of regional foreign trade, serving as a crucial foundation for government macroeconomic policies. Local general public budget revenues encompass the

allocation of funds for ensuring and enhancing livelihoods, fostering economic and social progress, safeguarding national security, and ensuring the smooth operation of national institutions, with tax revenue serving as the primary component.

A robust and balanced ecosystem is fundamental for cities to attain sustainable development and enhances the enhancement of cities' ecological resilience (ELR). Consequently, cities' disturbance resilience and ecosystem stability are evaluated through parameters such as industrial emissions, management of industrial waste, and urban self-purification capacity, including industrial wastewater and sulfur dioxide emissions, along with domestic waste management. The green coverage of urban districts reflects the ecological foundation and extent of green spaces, serving as a natural buffer against climate change and associated risks. Indicators such as industrial wastewater, sulfur dioxide, and industrial smoke emissions gauge pollution levels. Additionally, the comprehensive utilization rate of industrial solid waste and the safe disposal rate of domestic waste reflect pollution control effectiveness and the role of waste management and circular economy practices in emission reduction [62].

During a city's crisis, the resilience of basic infrastructure, including water, electricity, and transportation, is crucial, denoted as engineering resilience (EGR). Hence, five indicators—per capita water consumption, per capita electricity consumption, per capita liquefied petroleum gas (LPG) consumption, per capita road area, and the number of buses per 10,000 people—were selected to gauge urban residents' energy consumption and the level of urban infrastructure development. Water, electricity, and LPG consumption serve as negative indicators, reflecting higher energy consumption and thus greater vulnerability to shocks. Conversely, per capita road area and buses per 10,000 people signify the extent of urban infrastructure advancement, with larger values indicating better development of urban public infrastructure.

Table 2. The UR evaluation index system.

Criteria Layer	Indicator Layer	Indicator Attributes	Contents	References
Social Resilience (SR)	X_1: Population density	Person/km^2 (+)	Population distribution	[60]
	X_2: Number of college students per 1000 people	Person/1000 people (+)	Individuals' ability to cope with risk	[59]
	X_3: Number of people employed in the tertiary industry in the city	Person (+)	Social service capacity	[59,61]
	X_4: Number of patent applications	Items (+)	Future productivity of society	[63]
	X_5: Year-end urban registered unemployment rate	% (−)	Social stability capacity	[59]
Economic Resilience (ENR)	X_6: Gross regional product per capita	CNY (+)	Per capita economic strength	[53,60]
	X_7: Share of tertiary industry in GDP	% (+)	Industrial structure optimization level	[60,64]
	X_8: Per capita disposable income of urban residents	CNY (+)	Per capita consumption capacity	[64]
	X_9: Total import and export value	Billion USD (+)	Economic trade capacity	[60]
	X_{10}: Local general public budget revenue	Billion CNY (+)	Local government financial strength	[65]
Ecological Resilience (ELR)	X_{11}: Industrial wastewater emissions	10,000 t (−)	The disturbance power of industrial emissions to the city	[64]
	X_{12}: Industrial soot emissions	t (−)		[60,64]
	X_{13}: Industrial sulfur dioxide emissions	t (−)		[60]
	X_{14}: Harmless disposal rate of domestic waste	% (+)	The city's power to deal with industrial waste	[63]
	X_{15}: Comprehensive utilization rate of industrial solid waste (%)	% (+)		[60,65]
	X_{16}: Greening coverage rate of the jurisdiction (%)	% (+)	Self-purification capacity of the city	[60,66]
Engineering Resilience (EGR)	X_{17}: Per capita water consumption	t (−)	Energy consumption capacity of residents	[63]
	X_{18}: Electricity consumption per capita	kwh (−)		[63]
	X_{19}: LPG consumption per capita	t (−)		[60,67,68]
	X_{20}: Road area per capita	m^2/person (+)	Degree of infrastructure improvement	[59]
	X_{21}: Number of public buses per 10,000 people	Vehicles/10,000 people (+)		[65]

Notations: "(+)" represents positive indicators; "(−)" represents negative indicators.

2.2.4. Entropy-Weight-TOPSIS Evaluation Model

The entropy-weight TOPSIS evaluation model is a multi-criteria decision-making method that combines the TOPSIS model with the entropy method. This model is a

comprehensive evaluation approach based on the entropy-weight method to improve the TOPSIS model [69–74]. The principle is to detect the distance between the evaluated object and the optimal or worst values, subsequently calculating the proximity of the evaluated object to the ideal value and then ranking the strengths and weaknesses. The advantages of the entropy-weighted TOPSIS model are its ease of use, objectivity, minimal sample requirements, and the production of reasonable results [75]. Therefore, the entropy-weight TOPSIS evaluation model was used to assess the UR of the GBA in this study. By constructing the standardized matrix from the original data and defining the entropy method function, the entropy method can make full use of the information of the original data, calculate the indicator information utility value, and objectively carry out weight assignment. Then, the TOPSIS model was defined according to the matrix of weights obtained from the entropy weight method, and the resilience level of each city was obtained by calculating the Euclidean distance between the optimal and inferior ideal values by weighting the original values after each forwarding, which was used as the basis for the superiority or inferiority of the city's resilience. The larger the value is, the higher the level of comprehensive resilience of the city. The modeling steps are described below.

The entropy weighting method to determine the index weights is as follows:

$$w_j = \frac{1 - \mathrm{E}_j}{\sum_{j=1}^{\mathrm{n}} (1 - \mathrm{E}_j)}, \tag{4}$$

where w_j is the weight of indicator j, and E_j is the entropy value of indicator j.

The Euclidean distances between the target object and the superior and inferior solutions are calculated as follows:

$$\begin{aligned} r_j^+ &= \sqrt{\sum_{i=1}^{\mathrm{m}} \left[\mathrm{w}_i \left(\mathrm{o}_{ij} - \mathrm{o}_i^+\right)\right]^2} \\ \mathrm{r}_\mathrm{j}^- &= \sqrt{\sum_{i=1}^{\mathrm{m}} \left[\mathrm{w}_i \left(\mathrm{o}_{ij} - \mathrm{o}_i^-\right)\right]^2}, \end{aligned} \tag{5}$$

where o_i^+ is the optimal solution, o_i^- is the worst solution, o_{ij} is the value of the i-th evaluated object after the j-th evaluated index is normalized, and r_j^+ and r_j^- are the distances from each evaluated object to the optimal and worst solutions, respectively.

The comprehensive evaluation index, i.e., the evaluation index of the UR level, was calculated:

$$C_j = \mathrm{r}_j^- / \left(r_j^+ + \mathrm{r}_j^-\right), \tag{6}$$

where C_j is the closeness of the evaluated object to the optimal solution, and the larger the value is, the better the evaluated object is.

2.2.5. Spatial Autocorrelation Analysis Method

The Moran index can be used to measure spatial correlation, and this paper calculated the global Moran index of UR in the GBA by substituting the value of comprehensive UR into the following equation:

$$\text{Moran's I} = \frac{\sum_{i=1}^{\mathrm{n}} \sum_{j=1}^{\mathrm{n}} \mathrm{W}_{ij} (\mathrm{y}_i - \overline{\mathrm{y}}) \left(\mathrm{y}_j - \overline{\mathrm{y}}\right)}{\mathrm{s}^2 \sum_{i=1}^{\mathrm{n}} \sum_{j=1}^{\mathrm{n}} \mathrm{W}_{ij}}, \tag{7}$$

where y_i denotes the value of the urban toughness level in region i, $\overline{\mathrm{y}}$ is the mean value of urban toughness in the study area, s^2 is the variance of the urban toughness value, and W_{ij} denotes the spatial weight matrix. The value of the global Moran's index is in the interval of [–1,1]. The closer the value is to 0, the more likely the study area is in a random distribution state, and the larger the absolute value is, the more pronounced the spatial agglomeration of the study area.

The local Moran's I reflects the spatial heterogeneity and instability within the local area, which can be calculated as follows:

$$\text{Moran's } I_i = z_i' \sum_j w_{ij} z_j', \tag{8}$$

where z_i' and z_j' are the data after standardizing using the standard deviation, and W_{ij} is the standardized spatial weight matrix. When the value of the local Moran's index is less than 0, it indicates that the study area presents a state of spatial differentiation.

2.2.6. Coupling Coordination Degree Model

Coupling coordination is a concept from physics that refers to the interaction between different systems under the combined influence of themselves and the outside world [76]. As a method of analyzing the correlation between systems, it has gradually been applied in social sciences and other fields [77–79], and its calculation mainly consists of the coupling degree (C index) and the coordination degree (D index) [80]. The coupling degree mainly describes the degree of interconnection and interaction within multiple systems [81], measuring the degree of influence between two different systems on each other due to their own or external interactions. The higher the coupling, the stronger the connections and interactions between systems. Moreover, the coordination degree mainly captures the effect of coordinated development between systems [82], revealing synchronization and orderliness. The higher the coordination degree, the stronger the synergistic development effect of multiple systems. In the calculation, we introduced the coupling coordination index (D) to integrate the coupling degree and comprehensive coordination index, which can reflect the coupling degree and collaborative development status between two or more systems, effectively avoiding abnormal situations at low UHI and low UR levels, but can lead to the coordination of the two.

The coupling degree function of UHIs and UR is expressed as follows:

$$C = 2\{(u_1 u_2)/[(u_1 + u_2)(u_1 + u_2)]\}^{1/2}, \tag{9}$$

where C is the coupling degree, u_1 is the UHI subsystem, and u_2 is the UR subsystem.

For calculating the coordination degree and coupling coordination index of UHI and UR, the formula is as follows:

$$\begin{cases} D = (CT)^{1/2} \\ T = au_1 + bu_2 \end{cases}, \tag{10}$$

where C is the coupling degree; u_1 is the UHI subsystem; u_2 is the UR subsystem; D is the coupling coordination degree; T is the combined UHIs and UR reconciliation index, which reflects the overall synergistic effect or contribution of UHIs and UR; and a and b, which represent the contribution shares of UHIs and UR, respectively, are coefficients to be determined. This paper focused on the interrelationship between UR and HUIs by referring to other studies [80,83], and based on the general empirical method, UR is considered to be at the same level of importance as the UHI effect, so the coefficients a and b were both set to 0.5. In practical applications, it is preferable to make $T \in (0,1)$ so that $D \in (0,1)$ can be guaranteed for ease of use.

Based on the UHI proportion index, which reflects the UHI level, and the UR evaluation result, which reflects the resilience and recovery of a city, the coupling coordination degree model of UHIs and UR was constructed, and the coupling coordination degree index of UHIs and UR was obtained. The coupling coordination degree index was graded by referring to the grade classification criteria of the coupling coordination degree in the related literature (Table 3). According to the coordination level, from low to high, it was divided into 10 levels, i.e., extreme dysfunction, severe dysfunction, moderate dysfunction, mild dysfunction, near dysfunction, barely dysfunction, primary coordination, moderate extreme coordination, good coordination, and high-quality coordination, to analyze the coupling relationship and development stage of UHIs and UR.

Table 3. Coupling coordination degree classification standard.

D	D's Grade	D	D's Grade
$0.0 \leq D < 0.1$	Extreme disorder	$0.5 \leq D < 0.6$	Barely disorder
$0.1 \leq D < 0.2$	Severe disorder	$0.6 \leq D < 0.7$	Primary coordination
$0.2 \leq D < 0.3$	Moderate disorder	$0.7 \leq D < 0.8$	Moderate Coordination
$0.3 \leq D < 0.4$	Mild disorder	$0.8 \leq D < 0.9$	Good Coordination
$0.4 \leq D < 0.5$	Nearly disorder	$0.9 \leq D \leq 1.0$	High Coordination

2.2.7. Geographic Probe Model

Geodetectors are a set of statistical methods that detect spatial heterogeneity and reveal the driving forces behind it. One of the factor detectors is able to detect whether a factor has an impact on the variance of the spatial distribution of a certain indicator value by comparing the total variance of that certain geographic variable over different categories of subdivisions with the total variance of that variable over the whole study area, and its model is as follows:

$$q_{Y,h} = 1 - \frac{1}{N\sigma^2}\sum_{h=1}^{L} N_h \sigma_h^2, \quad (11)$$

where h = 1, 2, …, L is the factor to be measured, Y is the UR value, N_h is the number of detection factors, N is the number of evaluation units, and σ_h^2 and σ^2 are the variance of the indicator layer h and the Y value of the whole area, respectively. The q value takes the range of [0, 1], which is expressed as the explanatory power of the spatial variance of UR, and the larger the q value is, the stronger the explanatory power is.

In this paper, the factors that have been clearly identified as drivers of UHIs in existing studies (Table 4) are used in a Geodetector model to detect their influence on UR to further investigate which specific factors play a key role in the synergistic relationship between UHIs and UR.

Table 4. Influencing factor indicators.

Guideline Level	Indicator Level	Unit
Meteorological conditions	Y_1: Average temperature	°C
	Y_2: Precipitation	mm
	Y_3: Average wind speed	m/s
Greenhouse gas emissions	Y_4: Average CO_2 emissions	$kg/m^2/s$
Green space	Y_5: Green coverage of the district	%
Population distribution	Y_6: Population density	$person/km^2$
City size	Y_7: Average nighttime light intensity	/
Economic development	Y_8: Per capita gross regional product	CNY

There are many drivers of UHI formation, and the factors that have been shown to have a significant impact on the UHI level include meteorological conditions, greenhouse gas emissions, green space, population distribution, urban scale, and economic development, while UR is also influenced by a combination of urban social, economic, ecological, and engineering aspects. In this paper, from the above aspects of UHI drivers, eight indicators were selected, and geographic probes were introduced to detect the degree of influence of different indicators on the spatial differentiation of UR to reveal the influence mechanism of UHIs on UR in the GBA. The specific indicators were as follows: for meteorological conditions, average temperature, precipitation and average wind speed, which are the main indicators reflecting meteorological conditions, were selected; for greenhouse gas emissions, surface average CO_2 emissions were selected; for green space, the green coverage rate of the jurisdiction was used; for population distribution, population density was selected; and for urban scale, average nighttime light was used. In terms of economic development, the degree of GDP per capita was chosen for measurement.

2.3. Data Sources

In this paper, MODIS 8d synthetic surface temperature products MOD11A2 from 2000–2019 were selected, and the data are obtained from the NASA EARTHDATA website (https://earthdata.nasa.gov, accessed on 15 September 2022). MOD11A2 was provided by the MODIS sensor onboard the Terra satellite. The satellite has an 8-day period of synthetic surface temperature data, and the satellite transits over the study area at 10:30 a.m. and 22:30 p.m., with a spatial resolution of 1 km. These data are now widely used in studies related to urban thermal conditions and UHIs. Considering that there are more clouds and rain in the study area in spring and summer, resulting in more missing data, this paper selected MOD11A2 image data with high completeness during October–November in the autumn of 2000–2019 in the GBA to carry out the study; land use classification data were from the geographic monitoring cloud platform (www.dsac.cn/DataProduct, accessed on 1 May 2022); CO_2 emission data were from EDGAR—The Emissions Database for Global Atmospheric Research (https://edgar.jrc.ec.europa.eu/, accessed on 10 March 2022), with a spatial resolution of 1°; nighttime light brightness was calculated using the EANTLI-like annual nighttime light data from the Chinese long time series nighttime light dataset. Nighttime lighting data were with a spatial resolution of 1 km; the rest of the socioeconomic data were obtained from the statistical bureaus of cities in the GBA, and the missing data were supplemented using interpolation or substitution with the same type of indicators.

3. Results

3.1. Spatial and Temporal Evolution Characteristics of the UHIs

Red and orange in Figure 4 represent higher temperatures, mostly concentrated in the central regions of the GBA; green represents lower temperatures, mainly distributed in the northwest and northeast of the GBA and the surrounding areas in the southwest. Yellow represents the average temperature, forming a transition zone between the high-temperature areas and the low-temperature areas. From the distribution changes of each color in Figure 4, in 2000, the yellow transition zone was widely distributed in all parts of the GBA, while the red high-temperature zone and the green low-temperature zone were relatively small, indicating that the temperature of each region was similar at this time and the temperature distribution was more uniform. In 2005, the yellow transition zone squeezed the low-temperature zone, leading to a trend of overheating in the entire province. The red high-temperature zone spread in all directions until 2010, when it peaked, extending to the southwest and east of the GBA and forming a large high-temperature zone. Subsequently, the area of the high-temperature zone converged in 2015, and large areas in the northwest, northeast, and southwest were transformed into low-temperature areas. By 2019, the area of the yellow transition zone had shrunk significantly and had been replaced by the red high-temperature zone and the green low-temperature zone, indicating that urban temperatures in the GBA have been polarizing.

The spatial distribution of the UHPI levels in Guangdong, Hong Kong, and Macao was obtained by calculating the suburban temperature difference from October LST data of the GBA from 2000 to 2019 and dividing the UHIs into 1–5 levels, from weak to strong (Figure 5). The UHIs in the central region of the GBA are significantly higher than those in the surrounding areas, and the UHIs distribution is stable, with an overall trend of expansion in all directions over time. The UHI region forms a ring-shaped belt around the entrance of the Pearl River Delta with significant aggregation characteristics, and the strong UHIs are mainly distributed in the major cities, such as Foshan, Guangzhou, Dongguan, Shenzhen, Zhongshan, and Zhuhai, among which the intersection of Guangzhou, Foshan, and Zhongshan connects to form large and strong continuous UHIs, a phenomenon closely related to several factors, such as high urbanization, population concentration, and high percentage of floor area. The UHI-free and UHI-negative regions are mainly located in the northeast and southwest of the GBA, including Zhaoqing, Huizhou, Jiangmen, Hong Kong,

and northern Guangzhou, which have extensive vegetation coverage areas and can play a better cooling role.

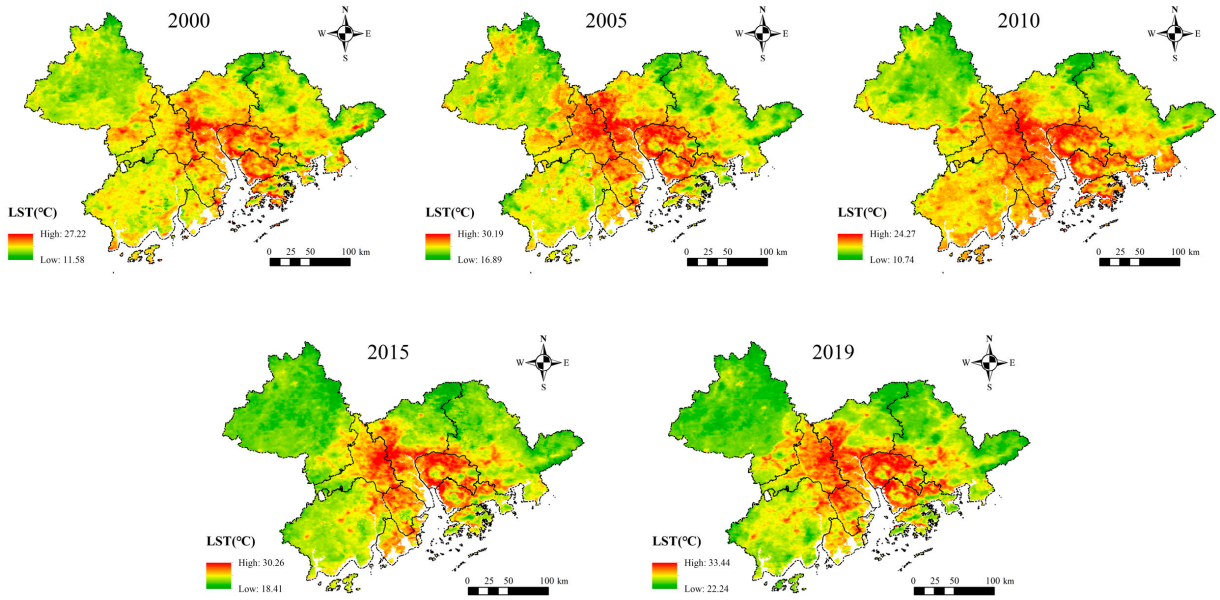


Figure 4. Spatial distribution of LST.

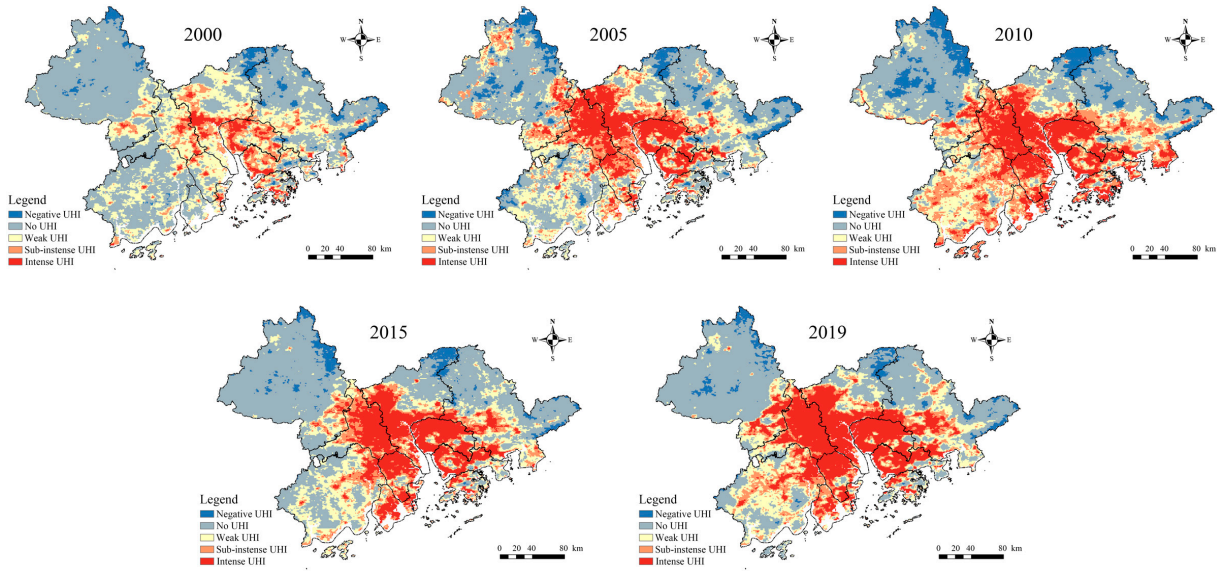


Figure 5. Spatial distribution of the UHIs.

Combining Figure 5 and accounting for the changes in the area and proportion of each UHI class (Figure 6a), it was found that the total UHI area in the GBA increased by 6743 km^2 between 2000 and 2019, and the percentage of UHI area increased from 40.46% in 2000 to 54.51% in 2019. Specifically, taking 2010 as a node, before 2010, the areas of strong UHIs, substrong UHIs, and weak UHIs in Guangdong, Hong Kong, and Macao continued to increase, with strong UHIs increasing the most, from 3.99% to 20.17%; the area of no UHIs shrank significantly, and the area of negative UHIs also increased. From 2011 to 2015, the areas of strong UHIs, substrong UHIs, and weak UHIs all decreased; the area of UHI-free increased back, and the area of negative UHIs also decreased. From 2016 to 2019, UHIs continued to expand, and the area of UHI-free and negative UHIs decreased.

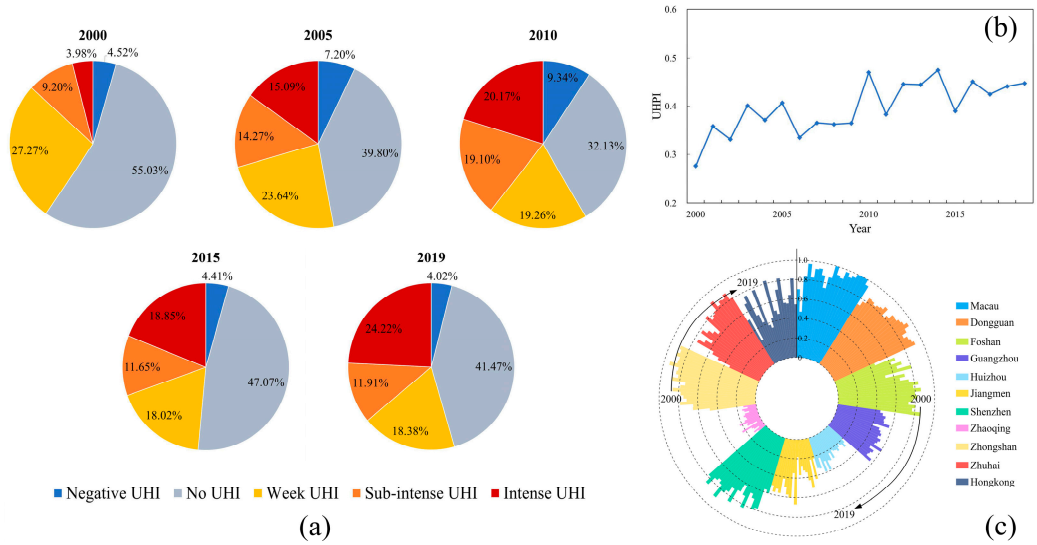


Figure 6. Change of UHI and UHPI. Notations: (**a**) is the area share of each UHI class; (**b**) is the results of the UHPI; (**c**) is the UHPI of cities.

By calculating the UHPI, the intensity of the UHI effect of each city in the study area was quantitatively reflected as a normalized index so that the UHI level could be quantitatively compared across time and across cities. Figure 6b shows the changes in the UHPI in the GBA from 2000 to 2019, and it can be observed that the UHPI of the GBA as a whole shows an increasing trend, indicating that its UHI degree is becoming more severe, with a 61.59% improvement in 2019 over 2000. Taking 2010 as the time node, during the period 2000–2010, the UHPI rose from 0.277 in waves to reach 0.470; during the period 2011–2019, the UHPI fluctuated by approximately 0.43, and the UHIs in the GBA had a tendency to gradually move towards stability.

At the city level (Figure 6c), the UHPI of all 11 cities in the study area showed a fluctuating upward trend from 2000 to 2019. Macao has the highest average UHPI, and its UHPI even reached 1 in 2010, indicating that Macao is completely covered by a UHI. This is followed by Dongguan, Zhongshan, Shenzhen, Zhuhai, and Foshan, all of which have maintained a UHPI of 0.7 or higher since 2010. Hong Kong, Guangzhou, and Jiangmen also have higher average UHI intensities, with Hong Kong and Jiangmen's UHI ratio indices varying significantly over the years, fluctuating sharply between 0.3 and 0.8 and 0.2 and 0.7, respectively, while Guangzhou has been relatively stable, ranging from 0.4 to 0.6. Zhaoqing has the lowest average UHPI, with its UHPI fluctuating roughly up and down in the 0.1 to 0.2 range, followed by Huizhou with a range of 0.2 to 0.4.

3.2. Spatiotemporal Change of UR in the GBA

Table 5 shows the UR levels of each city in the GBA in 2000, 2005, 2010, 2015, and 2019. The comprehensive UR scores of 11 cities are constantly improving, indicating that GBA's resistance and resilience to external shocks are becoming stronger. The cities with rapid UR development are distributed at the estuary of the Pearl River Delta and the area surrounded by Hong Kong, Macao, and the provincial capital Guangzhou, while the cities with slow UR development are located on the east and west sides separated by the Guangzhou-Hong Kong-Macao high UR belt. The development trend of UR in spatial distribution is from Hong Kong and Macao at the sea entrance to Shenzhen and the provincial capital Guangzhou and then develops towards the center from both ends, finally presenting the spatial distribution pattern of cities with high resilience in the regional centerline and cities, with low resilience on the east and west sides, which is discordant.

Table 5. The UR level of cities in the GBA.

Year	Macao	Dongguan	Foshan	Guangzhou	Huizhou	Jiangmen
2000	0.224	0.107	0.123	0.146	0.140	0.129
2005	0.248	0.103	0.112	0.176	0.136	0.123
2010	0.290	0.130	0.121	0.215	0.138	0.127
2015	0.365	0.180	0.141	0.283	0.147	0.128
2019	0.398	0.269	0.185	0.427	0.155	0.144
Year	**Shenzhen**	**Zhaoqing**	**Zhongshan**	**Zhuhai**	**Hongkong**	**Average**
2000	0.153	0.118	0.130	0.150	0.293	0.156
2005	0.180	0.119	0.125	0.151	0.323	0.163
2010	0.257	0.106	0.127	0.172	0.387	0.188
2015	0.380	0.120	0.140	0.193	0.434	0.228
2019	0.567	0.129	0.148	0.207	0.486	0.283

However, according to the graph of the evaluation scores of 11 cities in the GBA in the four sub-resilience dimensions (Figure 7), it was found that the development of cities in each sub-resilience dimension is obviously uneven. In terms of ELR, they are all at a high level, and over time, the difference in ELR between cities gradually narrows, indicating that the ecosystem in the region has strong resistance to external disturbances. Most cities within the GBA exhibit low resilience levels in SR and ENR, but significant growth in SR has occurred in Shenzhen and Guangzhou over the past 19 years, as well as high growth in ENR in Hong Kong, Macao, and Shenzhen. This indicates that the development of resilience to economic and social risk within the GBA is insufficient and uneven. In terms of EGR, Hong Kong has maintained a prominent high level for a long time, while the overall EGR levels of other cities are relatively close to medium-to-low levels, indicating that there is still room for improvement in the GBA's risk engineering facilities. Among them, Macao and Shenzhen have a faster growth rate. Overall, in recent years, almost all cities that have experienced rapid development in resilience were close to sea entrances. These cities have excellent ports or developed and convenient transportation conditions, as well as a special position in politics and economy. This may mean more active material and personnel mobility, as well as more flexible and loose policies, which are favorable conditions for the rapid development of resilience.

To explore the spatial clustering characteristics of the comprehensive UR in the GBA, a global spatial correlation analysis of the comprehensive resilience of the study area was conducted based on the Moran index, and the global Moran index of the comprehensive UR of the GBA was obtained for all years (Table 6). The Moran index of the UR in the GBA from 2000 to 2019 was positive, indicating that there was a positive spatial differentiation of the UR of the 11 cities in the GBA. Furthermore, UR in the GBA shows significant spatial clustering characteristics. The Moran index shows an increasing trend over time, indicating that the spatial agglomeration of UR in the GBA has been increasing.

Table 6. Global Moran index of UR.

Year	Moran's I	Year	Moran's I
2000	0.245	2010	0.303 *
2001	0.249	2011	0.315 *
2002	0.245	2012	0.326 *
2003	0.249	2013	0.333 *
2004	0.250	2014	0.331 *
2005	0.246	2015	0.343 *
2006	0.260	2016	0.334 *
2007	0.275 *	2017	0.345 *
2008	0.279 *	2018	0.311 *
2009	0.304 *	2019	0.320 *

Notations: * indicates that the hypothesis test was passed at the 10% significance level.

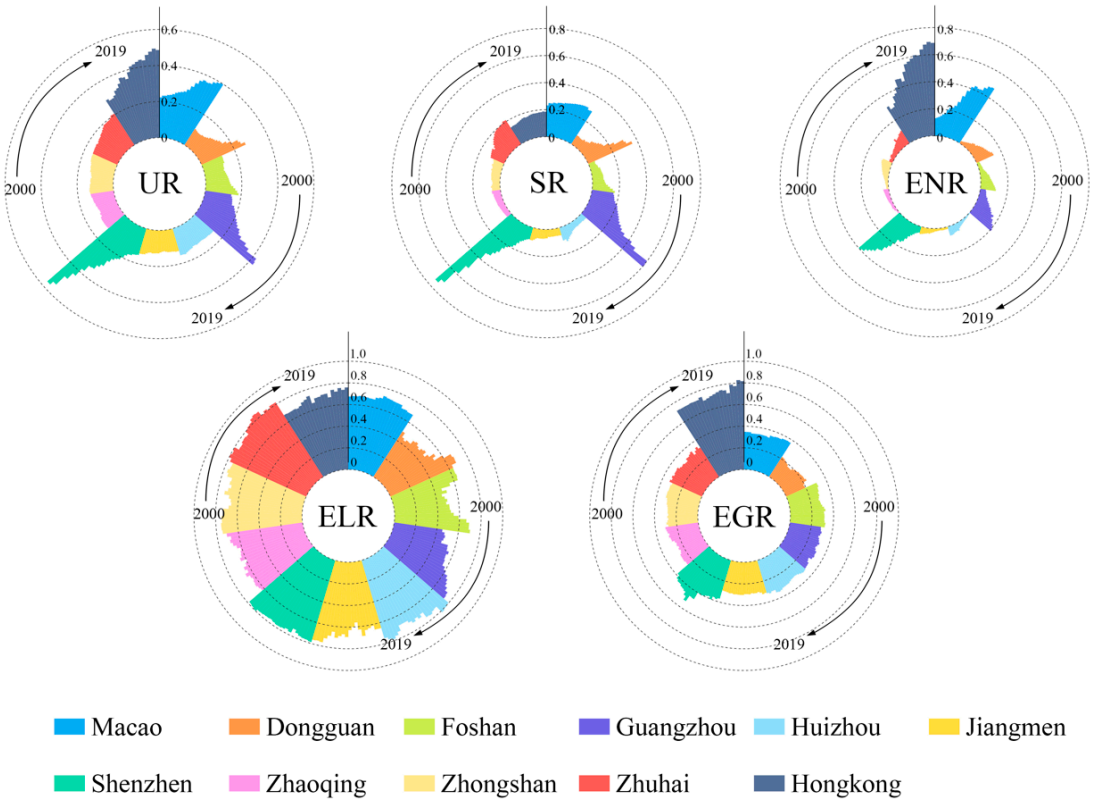


Figure 7. Different resilience dimensions of cities in the GBA.

To further show the local spatial relationship patterns of UR in the GBA and reveal the changing characteristics of local spatial autocorrelation of neighboring cities, the local Moran's I values of UR in the GBA for the years 2000, 2005, 2010, 2015, and 2019 were calculated using GeoDa1.12 platform , and LISA clustering maps were used for cities that passed the 5% significance test for performance (Figure 8). According to the LISA clustering map, it can be seen that there was a good local spatial autocorrelation of the integrated resilience of cities in the GBA from 2000 to 2019, indicating that the integrated resilience values among cities are more closely related spatially and that material functions are exchanged more frequently. The number of cities showing significant local autocorrelation has gradually increased over time. Low–low agglomeration type cities are distributed in the northwest inland fringe of GBA, including Zhaoqing and Foshan, while high–high aggregation type cities are distributed near the central bay and sea inlet of GBA, including Hong Kong, Macao, and Shenzhen. In 2000, 2015, and 2019, Zhuhai, Shenzhen, Dongguan, and Huizhou all showed a low–high aggregation type in succession, adjacent to the HK-Macao high–high aggregation area (which Shenzhen also joined after 2005), gradually developing a more and more significant low–high aggregation distribution northward, indicating that the gap between their resilience development level and the surrounding cities is increasing, and the surrounding cities with high resilience have not yet given full play to their radiation and driving role. The siphon effect exists between high–high aggregation areas and adjacent low–high aggregation areas, causing the necessary population, resources, economy, and other factors for the development of UR to continuously flow into high resilience areas from low resilience areas, exacerbating the aggregation and differentiation of resilience levels.

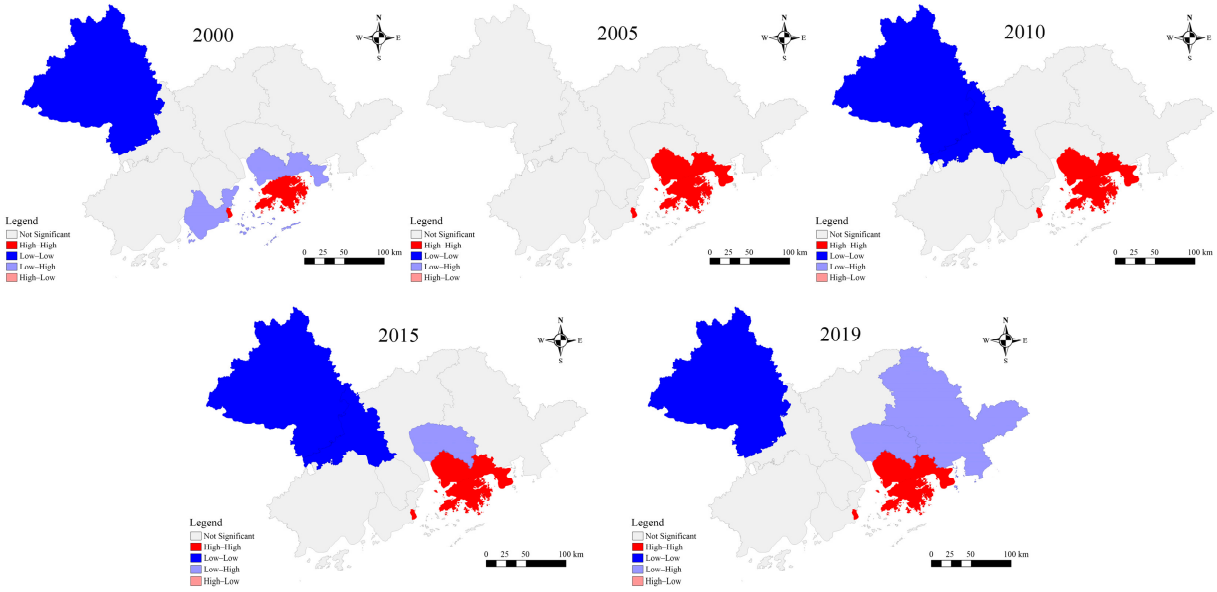


Figure 8. Local autocorrelation clustering of UR.

3.3. Coupling Coordination Analysis

From a qualitative perspective, UHIs have increased energy consumption and environmental pressure, causing impacts on multiple subsystems, such as urban ecology, society, and engineering. At the same time, the resilience development of each subsystem is based on economic growth, fair access to resources by citizens, new construction projects, and investment in environmental governance, which means more energy consumption and more intense human activities. Anthropogenic heat generation exacerbates UHIs, which are in a complex interactive coupling. In addition, the spatiotemporal trend characteristics of UHIs and UR indicate that both are clearly clustered in developed cities along the estuary in space, and there is a trend of expansion from these cities to the surrounding areas. However, it is uncertain to what extent there is interactive coupling between UHIs and UR. Therefore, this study uses quantitative methods to evaluate the degree of coupling between UHIs and UR and the comprehensive development level they collectively reflect.

The coupling degree © reflects the quantitative degree of co-variation between the UHI effect and UR, and a higher value indicates better coupling, which means that the closer the interaction between the two systems. As observed in Figure 9a, in the early stages of urbanization from 2000 to 2003, there was an obvious and continuous decrease in the coupling degree between UHIs and UR, indicating a weakened interaction between resilience development and UHIs during this stage. Similar situations occurred to varying degrees during the periods of 2008 to 2010 and 2011 to 2014. The coupling degree between UHIs and UR is high in all years, demonstrating the close interaction between UHIs and UR.

However, the C value only measures the degree of synergistic changes between different variables and cannot reflect the actual situation of UHIs and UR. When the scores of UHIs and UR subsystems are close, a highly coupled result will be obtained. This means that the changes between the two are highly synergistic but cannot provide information on whether the attribute level exhibited by UHIs and UR is high or low. In order to measure the degree of coupling between UHIs and UR while reflecting their common development status, we introduced a comprehensive coordination index (T) to describe the overall coordination effect or contribution of UHIs and UR, and a higher value indicates a better-coordinated development level. The calculated comprehensive coordination index of the UHI effect and UR is shown in Figure 9b, and it is found that the comprehensive coordination index shows a significant upward trend over time, indicating that UHIs and UR have generally maintained growth, with fluctuations and decreases during this period,

which means a reverse development of UHIs and UR in certain years. It has been noted that the coordination index has increased during the three time periods of 2000–2003, 2008–2010, and 2011–2014, while the coupling degree has decreased, indicating an uncoordinated development speed between UHIs and UR.

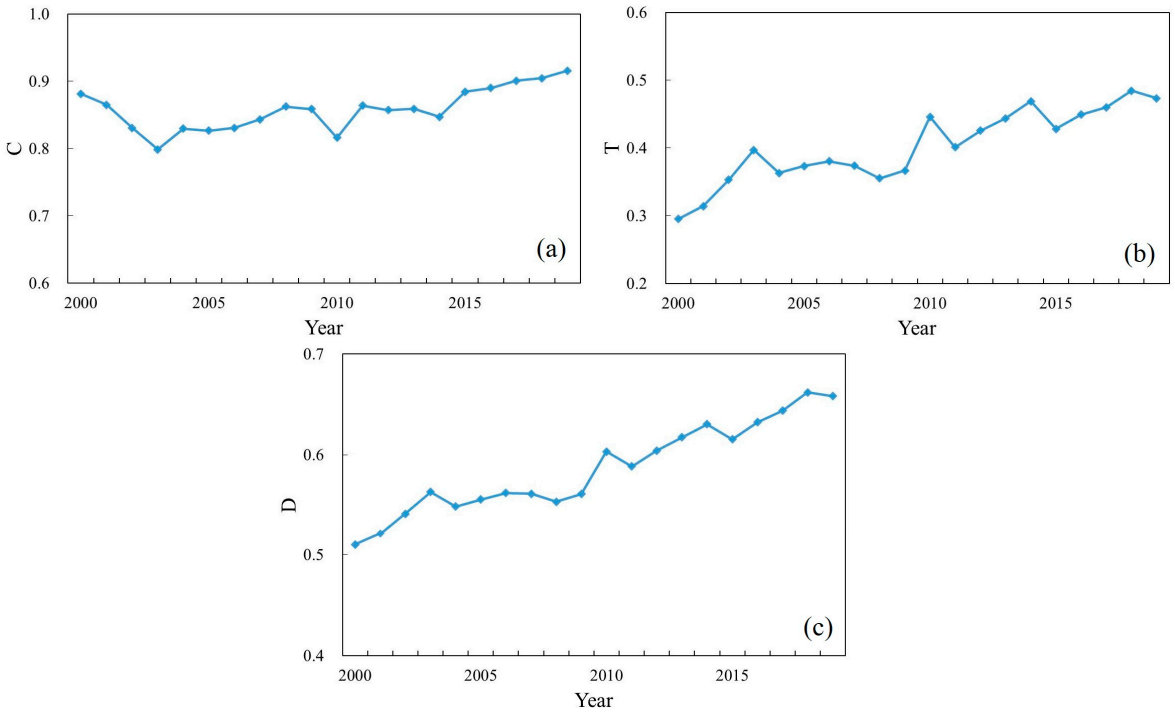


Figure 9. Results of the coupling coordination degree. Notations: (**a**) is the coupling degree index; (**b**) is the comprehensive coordination index; (**c**) is the coupling coordination degree between the UHI effect and UR.

The geometric average of the coupling degree and coordination index is used to calculate the coupling coordination degree to reflect the comprehensive level of close interaction and coordinated development between UHIs and UR. The results of the coupling coordination degree of the UHI effect and UR in the GBA were calculated as follows (Table 7 and Figure 9c). From 2000 to 2019, the coupling coordination degree of the UHIs effect and UR in the GBA showed a fluctuating upward trend. Taking 2010 as the node, the coupling coordination degree levels before 2010 were barely coordinated; moreover, 2010 was upgraded to primary coordination, and thereafter, it was basically maintained at primary coordination, indicating that although UHIs and UR are closely related, their comprehensive performance was not high before 2010, and the common development of UR and UHI did not produce a significant effect. After 2010, the coupling coordination degree developed to a certain extent, indicating that the corresponding cost of heat generation associated with the development of resilience has become increasingly apparent.

The results and spatial distribution of the coupling coordination degree between UHIs and UR of cities in Guangdong, Hong Kong, and Macao are described below (Table 8 and Figure 10). Before 2010, the coupling coordination degree in the study area was mainly on the verge of disorder and barely coordinated, and the growth rate of each city was slow; after 2010, the primary coordination and intermediate coordination gradually increased, and the growth rate of the coupling coordination degree in most cities increased.

Table 7. Coordination degree of coupling between the UHIs and UR.

Year	D	D's Grade	Year	D	D's Grade
2000	0.510	Barely coordinated	2010	0.603	Primary Coordination
2001	0.521	Barely coordinated	2011	0.589	Barely coordinated
2002	0.541	Barely coordinated	2012	0.604	Primary Coordination
2003	0.563	Barely coordinated	2013	0.617	Primary Coordination
2004	0.549	Barely coordinated	2014	0.630	Primary Coordination
2005	0.556	Barely coordinated	2015	0.615	Primary Coordination
2006	0.562	Barely coordinated	2016	0.632	Primary Coordination
2007	0.561	Barely coordinated	2017	0.644	Primary Coordination
2008	0.553	Barely coordinated	2018	0.662	Primary Coordination
2009	0.561	Barely coordinated	2019	0.658	Primary Coordination

Table 8. The coupling coordination degree between UHIs and UR coupling in cities in the GBA.

Cities	2000	2005	2010	2015	2019
Macao	0.629	0.692	0.734	0.769	0.783
Dongguan	0.528	0.542	0.582	0.634	0.706
Foshan	0.486	0.547	0.565	0.574	0.632
Guangzhou	0.506	0.563	0.572	0.607	0.702
Huizhou	0.407	0.424	0.450	0.452	0.475
Jiangmen	0.409	0.455	0.540	0.481	0.520
Shenzhen	0.550	0.588	0.683	0.734	0.816
Zhaoqing	0.322	0.409	0.362	0.318	0.362
Zhongshan	0.501	0.553	0.579	0.590	0.603
Zhuhai	0.476	0.555	0.615	0.632	0.640
Hongkong	0.625	0.610	0.753	0.704	0.716

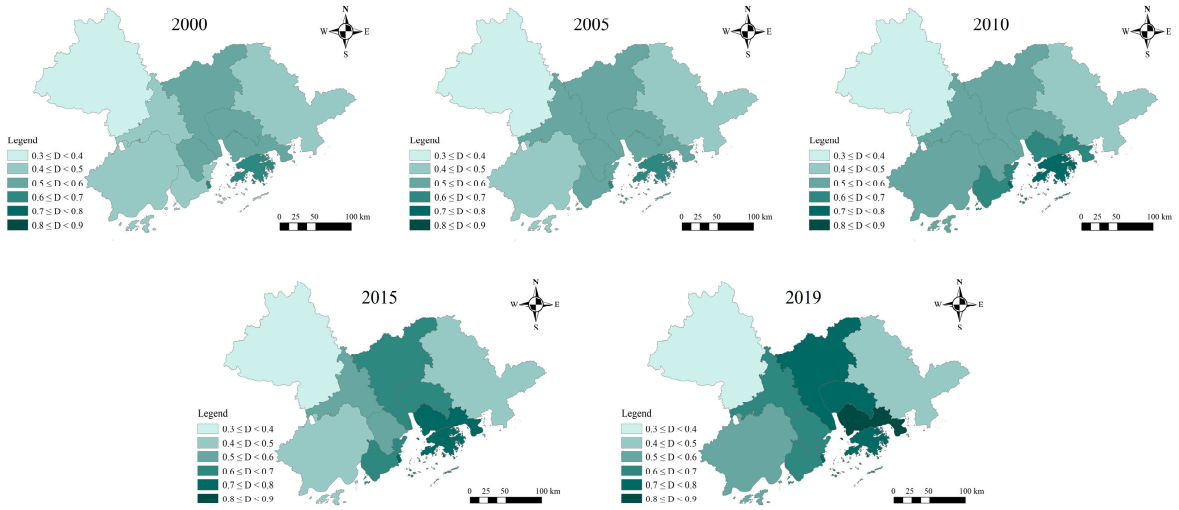


Figure 10. Spatial distribution of the coupling coordination degree of UHIs and UR in cities.

From the perspective of city location, the spatial distribution of the coastal cities in the center of the GBA showed a high degree of coupling coordination, while the coupling coordination degree gradually decreased in the north and east–west extension. Macao, Hong Kong, and Shenzhen have the highest coupling coordination degree, and all of them reached intermediate coordination after 2010, especially Shenzhen, which reached a good coordination level in 2018. The higher coupling coordination appears because their UHPI and UR scores are much higher than those of other cities, which indicates that the UHI effect is escalating significantly while UR is developing rapidly. The coupling coordination in Zhuhai, Dongguan, Guangzhou, Zhongshan, and Foshan gradually and steadily improved from a near-disorderly or barely coordinated state in 2000 to a primary coordination or even

intermediate coordination level in 2019. In these cities, the UHPI and UR scores also remain high, indicating that the development of UHIs and UR shows some synergistic effects. Zhaoqing, Huizhou, and Jiangmen have a low average coupling coordination degree and are basically below barely a disorder, and their UHPI and UR scores are low in the GBA.

3.4. The Interaction Mechanism between the Heat Island Effect and Urban Resilience

During the period 2000–2019, each factor showed different degrees of influence on the UR of the GBA (Table 9). The four indicators with strong average explanatory power for the spatial differentiation of UR in the selected years are GDP per capita, population density, average precipitation and nighttime light brightness. Among them, the average explanatory power of GDP per capita and population density was 0.761 and 0.760, respectively; their influence was almost similar, and their q-values both developed from approximately 0.6 in 2000 to approximately 0.8 in 2019, which reflects the degree of urban economic development and the release of anthropogenic heat, respectively, suggesting that both have a greater explanatory power for the spatial differentiation of UR in the GBA. Average precipitation is one of the meteorological conditions, and its explanatory power on UR is also high, with an average explanatory power of 0.594, so it also needs to be emphasized in studies on improving UR. The average explanatory power of this indicator is 0.489, which shows a fluctuating upward trend, indicating that the difference in urban scale in the GBA is gradually expanding and has a correlation with UR.

Table 9. Influence of each factor on UR.

Variables	2000	2005	2010	2015	2019
Y_1	0.235	0.358	0.626	0.348	0.093
Y_2	0.634	0.707	0.256	0.876	0.498
Y_3	0.614	0.190	0.279	0.261	0.495
Y_4	0.371	0.514	0.455	0.307	0.402
Y_5	0.387	0.069	0.281	0.355	0.047
Y_6	0.626	0.689	0.800	0.876	0.808
Y_7	0.314	0.358	0.286	0.876	0.613
Y_8	0.614	0.190	0.279	0.261	0.495

The data for 2000, 2005, 2010, 2015, and 2019 were selected, and geographic probes were used to further detect the comprehensive relationship between the four dimensions of the sub-resilience systems by the drivers of UHIs (Figure 11). In 2000, the spatial differentiation of ENR could be most explained by the drivers of UHIs, among which population density and precipitation had a greater explanatory power on SR. In 2005, the explanatory power of each factor on the spatial variation of SR was stronger, among which the higher explanatory power was the per capita gross regional product and precipitation, indicating that the economic development and precipitation in the meteorological conditions had a greater explanatory power on SR in that year; the remaining resilience dimensions in the order of the degree of explanatory power were SR, EGR, and ELR. In 2010, ELR could be best explained by the combination of all factors, among which population density and the average temperature had the strongest explanatory power, and this year was also the time when the UHI effect was more serious, indicating that the higher temperature of anthropogenic heat emission had a correlation with urban ELR in this year; the remaining resilience dimensions were ENR, EGR, and ELR in descending order of explanatory power. In 2015, all four resilience dimensions could be explained by the drivers of the UHI effect, with precipitation and population density having a greater explanatory power on both sub-resilience types of ENR and ELR. In 2019, ENR could be mostly explained, with GDP per capita and population density having a higher explanatory power on ENR and precipitation; the remaining resilience dimensions were SR, ELR, and EGR according to the explanatory power from largest to smallest.

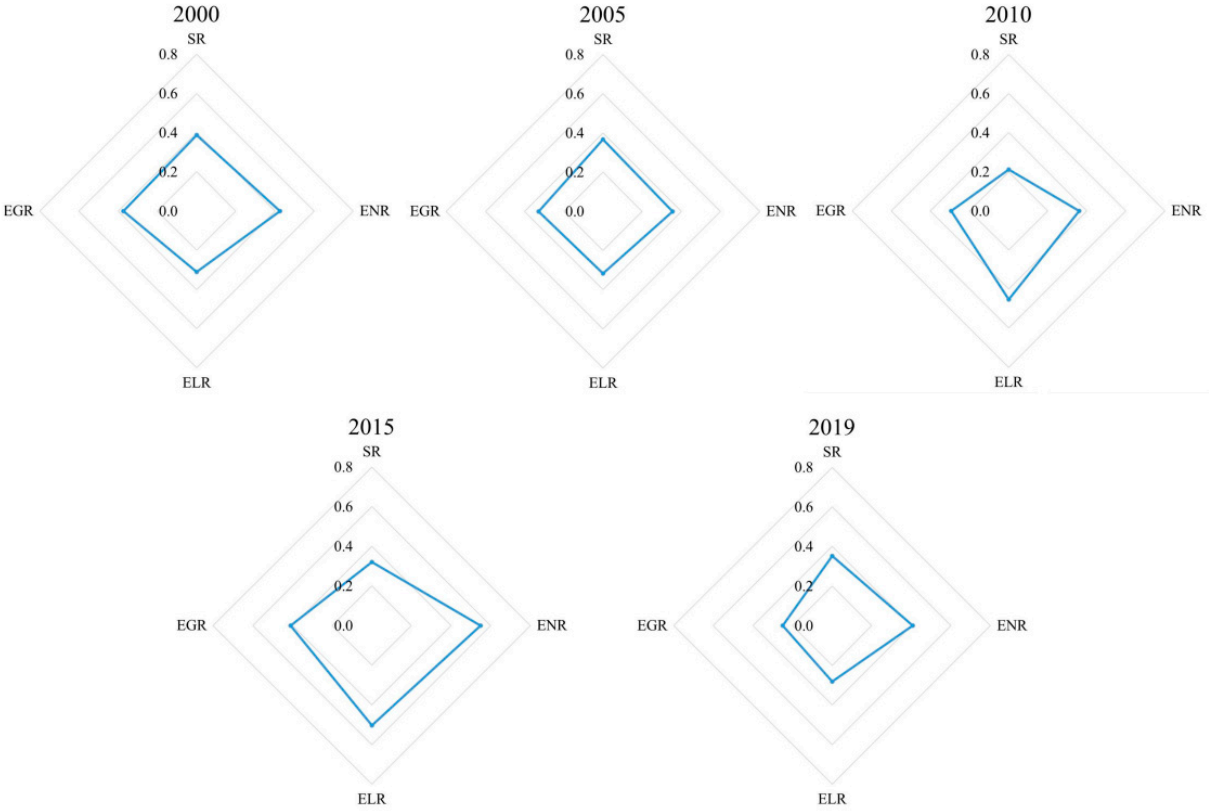


Figure 11. Dimensional resilience impact.

To further explore the mechanism of the drivers of the UHIs interacting with UR, interaction detection in Geodetector was used to analyze the data in the GBA in 2000, 2005, 2010, 2015, and 2019 to assess whether the influencing factors, when acting together, increase or weaken the explanatory power of UR, and the results are shown in Figure 12. The interaction mechanism between factors is dominated by two-factor enhancement, with nonlinear enhancement as a minority, and there is no independent or weakening effect, indicating that the interaction between two factors has a stronger effect on the spatial distribution of UR than the single-factor effect. The top four strongest interactions with other factors are GDP per capita, per capita CO_2 emissions, population density, and precipitation. From 2000 to 2010, the interaction of per capita CO_2 emissions was the most prominent, and in 2015, GDP per capita became the strongest interacting factor, and in 2019, the most obvious interaction effect was population density. Specifically, the four pairs of factors with the strongest interaction in 2000 were green cover and wind speed, green cover and GDP per capita, per capita CO_2 emissions and wind speed, and per capita CO_2 emissions and GDP per capita, while the three pairs of factors with the strongest interaction in 2005 were green cover and precipitation, per capita CO_2 emissions and wind speed, and green cover and GDP. In 2010, the three strongest two-factor interactions were land-averaged CO_2 emissions versus temperature, land-averaged CO_2 emissions versus population density, and land-averaged CO_2 emissions versus precipitation. In 2015, the three strongest two-factor interactions were GDP per capita versus temperature, GDP per capita versus population density, and GDP per capita versus nighttime brightness. In 2019, the three strongest two-factor interactions were precipitation and population, precipitation and nighttime light brightness, and precipitation and GDP per capita. It is thus found that the factors of GDP per capita, population density, and precipitation, which are individually more influential on the spatial differentiation of UR, are also more influential in terms of their interactions. Although the influence of per capita CO_2 emissions is not strong by itself, it becomes stronger when it interacts with other factors, and its interaction was very important before 2010.

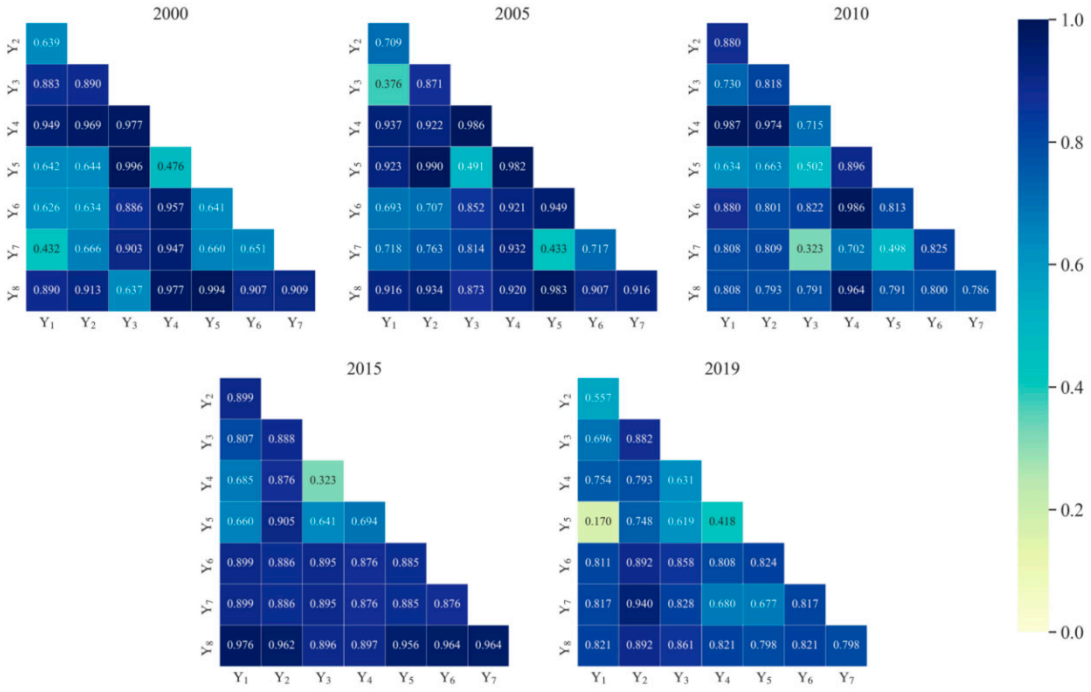


Figure 12. Interactive detection results of the geographic detector.

4. Discussion

China is facing many problems in the process of urbanization, with various uncertain impacts such as climate change and natural disasters threatening the smooth operation of urban system functions. Urban disaster resilience is a new urban risk management method that allows cities to continuously adapt to external environmental changes and reduce the risks brought about by uncertainty [84]. With the intensification of human activities [19–21] and the artificial transformation of nature [85], the urban environment is more prone to generating abnormally high temperatures [86], causing pressure on urban energy, the environment, and residents' health. Previous studies have often focused on the formation and prediction of UHIs, with little attention paid to the attributes of urban systems that maintain and restore their original state under the influence of UHIs. The consideration of the interaction between UHIs and the functions of urban subsystems is also limited. This study established a framework to evaluate the spatiotemporal evolution characteristics of UHIs and UR over a period of time and quantitatively evaluated the close connection between UHIs and UR using a coupling coordination model. We further investigated the role of driving factors of UHIs in the spatial differentiation of UR using geographic detectors.

The results show that the UHI phenomenon and high UR level in the GBA are mainly concentrated in the coastal areas near the Pearl River Delta estuary, and their levels have been rising in the past two decades, with a trend of diffusion to the surrounding areas. This is consistent with the conclusion that the resilience level and UHIs of most cities in China have been increasing year by year over the past two decades [87,88] and are in line with the development path of cities in GBA. In the early stages of development, Hong Kong and Macao, which experienced colonial times, already had a good economic foundation, allowing their economic functions to better adapt to risks. Hong Kong also retained high-level infrastructure, giving it better reconstruction potential after disasters. Shenzhen, as an important city in GBA, is adjacent to Hong Kong and Macao and can take on their driving role well. It is also one of the fastest developing cities in the GBA, and Guangzhou, as the provincial capital, has received good policy support. They can attract a large influx of population, making their internal social structure more dynamic and variable. It is worth noting that the uneven development of resilience levels between cities

is closely related to the economic vitality and social diversity of the cities themselves [60]. The cities that develop first benefit from the advantages of population, resources, and production capacity, exacerbating the differentiation of social resource possession and development level. Therefore, in order to avoid the negative siphon effect of first-mover cities on the resilient development of surrounding cities, the GBA government should encourage industrial cooperation and coordinated development between different regions, promote industrial transfer and upgrading through policy guidance and support, form a complementary industrial system, and enhance population attractiveness and stickiness. In addition, establish effective coordination mechanisms, including consultation meetings and cooperation forums between different regions, strengthen communication, coordination, and cooperation, deepen regional integration, promote resource flow, and strengthen regional coordinated development to promote regional synergy. Taking megacities as the center, building satellite cities in the surrounding areas, evacuating and undertaking population, technology, and industrial transfers from centrally developed cities, replacing some functions of central cities, and achieving polycentric urban construction.

The research on the coupling and coordination of UHIs and UR shows that there is an obvious coupling relationship between the two. Especially in the cities at the estuary of the Pearl River Delta, UHIs and UR maintain a highly synchronized change and continuous development trend. However, their development speed is sometimes not coordinated during this process. Due to the fact that the early and middle stages of urban development are often driven by intensive industries, we believe that this lack of coordination is caused by low efficiency in resource and energy utilization and UR development is accompanied by excessive heat generation. The results also indicate that among the driving factors of UHI formation, economic development, population distribution, greenhouse gas emissions, and urban size are correlated with the spatial differentiation of UR. Therefore, the government should adopt the following strategies to promote the development of UR while mitigating UHIs.

Green vegetation coverage is considered the most effective measure for UHIs [89]. By issuing green policies, organizing tree planting, establishing parks and green belts, and constructing rooftop gardens to increase shade and evapotranspiration, thereby achieving cooling and absorbing carbon dioxide, effectively reducing the aftereffect of energy consumption during urban development. In addition, improving urban ventilation can reduce LST and mitigate the impact of UHI [90–92]. Finally, we should adjust the industrial structure, encourage enterprises to develop advanced green technologies, promote the green and low-carbon transformation of the industry, cultivate and strengthen low-carbon, zero-carbon, and negative-carbon industries, promote renewable energy and improve energy efficiency, and generate as little heat production cost as possible while ensuring development.

In the future, cities will still face various climate change threats, including UHIs, and there are complex interactive impact mechanisms. In the development process of resilience and other attributes in urban systems, there is shortsightedness caused by cognitive limitations. The uncertainty of risk shocks determines that managers and citizens cannot guarantee recognition of all unforeseeable disasters or all potential risk factors and cannot guarantee that seemingly good resilience levels can cope with all types of sudden risks. If the development of UR only focuses on the integrity, resilience, and adaptability of the urban form itself, it is not enough. For those risks that appear outside the existing resilience goals, urban risk emergency management is particularly important. The GBA government should accelerate the development of climate action plans, conduct corresponding risk assessments, identify the main threats faced by cities, and develop strategies and measures for mitigation and adaptation, including improving agricultural technology, strengthening flood control mechanisms, improving urban pipeline systems, water conservation and recycling. In addition, regional integrated action planning across administrative regions should be promoted to provide a globally coordinated response to climate change. Small and medium-sized innovative enterprises should be supported to promote economic di-

versity. Emergency reserve funds should be established, various basic social insurances improved, flexible employment policies implemented, and employment opportunities created. Furthermore, regular assessments are conducted on urban construction facilities to identify potential risk factors and check for potential hazards in roads, bridges, and water supply and power systems. Emergency response plans should be developed to ensure that the normal functioning of urban construction and facilities can be restored as soon as possible after a hazard occurs. Traffic and transportation management should be optimized, backup transportation routes should be increased, and open spaces for emergency evacuation should be built to ensure the mobility of materials and personnel. The construction of smart cities should be encouraged, real-time intelligent and automated services in transportation, logistics, healthcare, and other fields should be provided, and the maintainability of infrastructure should be improved.

5. Conclusions

In this study, we proposed a methodological framework for unveiling the coupling coordination and interaction mechanism between UHIs and UR. On this basis, we explored the spatiotemporal evolution trend, coupling coordination, and the correlation of spatial differentiation of UHIs and UR in various cities within GBA. Eleven cities of the GBA in China were used as the study area for research discussions and results analysis. The main conclusions are as follows:

(1) From 2000 to 2019, the UHI region of the GBA formed a ring-shaped belt around the entrance of the Pearl River Delta, with strong UHIs mainly distributed in the major cities, such as Foshan, Guangzhou, Dongguan, Shenzhen, Zhongshan, and Zhuhai. The UHIs in the GBA show a significant trend of expansion and escalation over time, with Jiangmen's UHI area expanding the most and Macao's expanding the least; Macao has the highest average UHPI, and Zhaoqing has the lowest average UHPI.

(2) The cities with rapid development of UR in the GBA were distributed in the ring of the Pearl River Delta inlet, and the cities with slow development were distributed in the vicinity, finally showing the spatial distribution pattern of high resilience of the regional central cities and low resilience of the peripheral cities, and the development of the resilience level of each city shows an uncoordinated trend. High–high aggregation type cities are distributed near the central bay and sea inlet of GBA. Adjacent to the HK-Macao high–high aggregation area, a more and more significant low-high aggregation distribution is gradually developing northward.

(3) The coupling degree between UHIs and UR is high in all years, demonstrating the close interaction between UHIs and UR. Before 2010, the coupling coordination degree of the study area was mainly on the verge of disorder and barely coordinated, and the growth rate of each city was slow; in 2010 and after, the primary coordination and intermediate coordination gradually increased, and the growth rate of the coupling coordination degree in most cities increased, indicating that the common effect of UHIs and UR development is becoming increasingly significant. From the viewpoint of city location, the spatial distribution of coastal cities in the center of the GBA shows a high degree of coupling coordination, while the coupling coordination decreases gradually in the north and east–west extension.

(4) Among the drivers of UHIs, GDP per capita, population density, land-average CO_2 emissions, and average nighttime light brightness have stronger explanatory power for the spatial variation in UR. The spatial differentiation of the four sub-dimensions of UR is related to the driving factors of UHIs to varying degrees. The interaction between two factors has a stronger explanatory power for the spatial distribution of UR than a single factor.

There are various potential limitations of this study. First, the selection of the UR evaluation index system and UR impact factor index system in this paper is not sufficiently comprehensive, and the research and analysis of the indices are not sufficiently deep.

Second, only MODIS data were used for the selection of remote sensing data, and more accurate and comprehensive information could be obtained if multisource remote sensing data were used. Third, the situation under the influence of the new coronavirus epidemic after 2020 was not considered in the study period. Finally, we found that there is indeed a correlation between UHIs and UR, and this correlation may be hierarchical; that is, certain driving factors when UHIs occur also interact with UR. This indicates the complexity of the interaction between the two, but the details of this complexity still need to be further validated. We believe that more detailed theoretical assumptions and some structural model tests, as well as the introduction of causal inference methods, may be needed in our next research to help find appropriate entry points for intervention and fine control of the heat island phenomenon and UR levels.

Author Contributions: Conceptualization, H.W.; Data curation, S.L., H.X., T.X., W.H., X.G. and R.J.; Formal analysis, Y.Y. and S.L.; Funding acquisition, H.W.; Investigation, S.L.; Methodology, H.W., Y.Y. and S.L.; Project administration, H.W.; Visualization, Y.Y., S.L., H.X., T.X., W.H. and X.G.; Writing—original draft, H.W., Y.Y. and S.L. All authors have read and agreed to the published version of the manuscript.

Funding: This research was financially supported by the National Natural Science Foundation of China (No. 42201241), the National Key Research and Development Project of China (No. 2021YFC3101700), the Supplemental Funds for Major Scientific Research Projects of Beijing Normal University, Zhuhai (No. ZHPT2023001), and the startup fund to Huihui Wang from Advanced Institute of Natural Sciences, Beijing Normal University at Zhuhai (No. 310432104).

Institutional Review Board Statement: Not applicable.

Informed Consent Statement: Not applicable.

Data Availability Statement: The data used to support the findings of this study will be made available by the corresponding authors upon request.

Acknowledgments: The authors would like to thank the anonymous reviewers for their helpful and constructive comments.

Conflicts of Interest: The authors declare no conflicts of interest.

References

1. Reia, S.M.; Rao, P.S.C.; Barthelemy, M.; Ukkusuri, S.V. Spatial structure of city population growth. *Nat. Commun.* **2022**, *13*, 5931. [CrossRef]
2. Parham, A.M.; Fariborz, H. Approaches to study Urban Heat Island—Abilities and limitations. *Build. Environ.* **2010**, *45*, 2192–2201.
3. Peter, S. How climate change affects extreme weather events. *Science* **2016**, *352*, 1517–1518.
4. Saahil, S.; Dimitry, G.; Kevin, E.T.; Steven, C. Trends of extreme US weather events in the changing climate. *Proc. Natl. Acad. Sci. USA* **2022**, *119*, e2207536119.
5. Zhang, Y.; Yang, P.; Gao, Y.; Leung, R.L.; Bell, M.L. Health and economic impacts of air pollution induced by weather extremes over the continental U.S. *Environ. Int.* **2020**, *143*, 105921. [CrossRef]
6. Chen, Z.; Gong, Z.; Yang, S.; Ma, Q.; Kan, C. Impact of extreme weather events on urban human flow: A perspective from location-based service data. *Comput. Environ. Urban Syst.* **2020**, *83*, 101520. [CrossRef]
7. Kayaga, S.M.; Amankwaa, E.F.; Gough, K.V.; Wilby, R.L.; Abarike, M.A.; Codjoe, S.N.A.; Kasei, R.; Nabilse, C.K.; Yankson, P.W.K.; Mensah, P.; et al. Cities and extreme weather events: Impacts of flooding and extreme heat on water and electricity services in Ghana. *Environ. Urban* **2021**, *33*, 131–150. [CrossRef]
8. Zou, X.Y.; Peng, X.Y.; Zhao, X.X.; Chang, C.P. The impact of extreme weather events on water quality: International evidence. *Nat. Hazards* **2023**, *115*, 1–21. [CrossRef]
9. Voogt, J.A.; Oke, T.R. Thermal remote sensing of urban climates. *Remote Sens. Environ.* **2003**, *86*, 370–384. [CrossRef]
10. Neha, Y.; Chhemendra, S.; Peshin, S.K.; Renu, M. Study of intra-city urban heat island intensity and its influence on atmospheric chemistry and energy consumption in Delhi. *Sustain. Cities Soc.* **2017**, *32*, 202–211.
11. Haider, T. Meteorological, air-quality, and emission-equivalence impacts of urban heat island control in California. *Sustain. Cities Soc.* **2015**, *19*, 207–221.
12. Peter, K.; Sarah, L.; Angela, H. Evidence of urban heat island impacts on the vegetation growing season length in a tropical city. *Landsc. Urban Plan.* **2021**, *206*, 103989.

13. Arsad, F.S.; Hod, R.; Ahmad, N.; Ismail, R.; Mohamed, N.; Baharom, M.; Osman, Y.; Radi, M.F.M.; Tangang, F. The impact of heatwaves on mortality and morbidity and the associated vulnerability factors: A systematic review. *Int. J. Environ. Res. Public Health* **2022**, *19*, 16356. [CrossRef]
14. Gallo, K.P.; Mcnab, A.L.; Karl, T.R.; Brown, J.F.; Tarpley, J.D. The use of NOAA AVHRR data for assessment of the urban heat island effect. *J. Appl. Meteorol.* **1993**, *32*, 899–908. [CrossRef]
15. Li, Y.M.; Zhang, J.H.; Gu, R.Z. Study on the relationship between urban greening and heat island effect in Beijing. *China Gard.* **2004**, *2004*, 77–80.
16. Tong, H.; Liu, H.Z.; Li, Y.M.; Sang, J.G.; Hu, F. Current status of urban heat island in Beijing in summer and the role of wedge-shaped green space planning for urban heat island mitigation. *J. Appl. Meteorol.* **2005**, *2005*, 357–366.
17. Zhou, D.; Zhang, L.; Li, D.; Huang, D.; Zhu, C. Climate–vegetation control on the diurnal and seasonal variations of surface urban heat islands in china. *Environ. Res. Lett.* **2016**, *11*, 074009. [CrossRef]
18. Hu, F.; Liu, X.M.; Li, L.; Wang, Y. Summer urban climate trends and environmental effect in the Beijing area. *Chin. J. Geophys.* **2006**, *49*, 617–626. [CrossRef]
19. Peng, S.; Piao, S.; Ciais, P.; Friedlingstein, P.; Ottle, C.; Nan, H.; Zhou, L.; Myneni, R.B. Surface urban heat island across 419 global big cities. *Environ. Sci. Technol.* **2012**, *46*, 696–703. [CrossRef]
20. Wang, J.; Huang, B.; Fu, D.; Atkinson, P.M. Spatiotemporal variation in surface urban heat island intensity and associated determinants across major Chinese cities. *Remote Sens.* **2015**, *7*, 3670–3689. [CrossRef]
21. Zhou, D.C.; Zhang, L.X.; Hao, L.; Sun, G.; Liu, Y.Q.; Zhu, C. Spatiotemporal trends of urban heat island effect along the urban development intensity gradient in China. *Sci. Total Environ.* **2016**, *544*, 617–626. [CrossRef]
22. Foley, J.A.; Defries, R.; Asner, G.P.; Barford, C.; Bonan, G.; Carpenter, S.R.; Stuart Chapin, F.; Coe, M.T.; Daily, G.C.; Gibbs, H.K.; et al. Global consequences of land use. *Science* **2005**, *309*, 570–574. [CrossRef] [PubMed]
23. Zhao, L.; Lee, X.; Smith, R.B.; Oleson, K. Strong contributions of local background climate to urban heat islands. *Nature* **2014**, *511*, 216–219. [CrossRef] [PubMed]
24. Estrada, F.; Botzen, W.J.W.; Tol, R.S.J. A global economic assessment of city policies to reduce climate change impacts. *Nat. Clim. Chang.* **2017**, *7*, 403–406. [CrossRef]
25. Li, D.; Liao, W.; Rigden, A.J.; Liu, X.; Wang, D.; Malyshev, S.; Shevliakova, E. Urban heat island: Aerodynamics or imperviousness? *Sci. Adv.* **2019**, *5*, eaau4299. [CrossRef]
26. Cheng, H.; Yang, G.L.; Ji, X.J. A study on decoupling relationship between urban toughness and environmental pressure in China's top ten city agglomerations. *Stat. Decis. Mak.* **2019**, *35*, 79–83. (In Chinese)
27. Ahem, J. From fail-safe to safe-to-fail: Sustainability and resilience in the new urban world. *Landsc. Urban Plan.* **2011**, *100*, 341–343.
28. Foster, H.D. *The Ozymandias Principles: Thirty-One Strategies for Surviving Change*; UBC Press: Victoria, BC, Canada, 1997.
29. Etkin, D. Risk Transference and Related Trends: Driving Forces Towards More Mega-disasters. *Environ. Hazards* **1999**, *1*, 69–75.
30. Mileti, D.S. *Disasters by Design: A Reassessment of Natural Hazards in the United States*; Joseph Henry Press: Washington, DC, USA, 1999.
31. Holling, C.S. Resilience and stability of ecological systems. *Annu. Rev. Ecol. Syst.* **1973**, *4*, 1–23. [CrossRef]
32. Perrings, C. Resilience in the dynamics of economy-environment systems. *Environ. Resour. Econ.* **1998**, *11*, 503–520. [CrossRef]
33. Walker, B.; Hollin, C.S.; Carpenter, S.R.; Kinzig, A. Resilience, adaptability and transformability in social-ecological systems. *Ecol. Soc.* **2004**, *9*, 5. [CrossRef]
34. Martin, R.; Sunley, P.; Gardiner, B.; Tyler, P. How regions react to recessions: Resilience and the role of economic structure. *Reg. Stud.* **2016**, *50*, 561–585. [CrossRef]
35. Daniel, F.G. Mental resilience: Progress and prospects. *Curr. Opin. Psychol.* **2017**, *16*, 17–23.
36. Masten, A.S.; Obradović, J. Disaster preparation and recovery: Lessons from research on resilience in human development. *Ecol. Soc.* **2008**, *13*, 9. [CrossRef]
37. Crowe, P.R.; Foley, K.; Collier, M.J. Operationalizing urban resilience through a framework for adaptive co-management and design: Five experiments in urban planning practice and policy. *Environ. Sci. Policy* **2016**, *62*, 112–119. [CrossRef]
38. Shao, Y.W.; Xu, J. Understanding urban resilience: A conceptual analysis based on integrated international literature review. *Int. Urban Plan.* **2015**, *30*, 48–54. (In Chinese)
39. O'Malley, C. Urban Heat Island (UHI) mitigating strategies: A case-based comparative analysis. *Sustain. Cities Soc.* **2015**, *19*, 222–235. [CrossRef]
40. Carvalho, D.; Martins, H.; Marta-Almeida, M.; Rocha, A.; Borrego, C.J.U.C. Urban resilience to future urban heat waves under a climate change scenario: A case study for Porto urban area (Portugal). *Urban Clim.* **2017**, *19*, 1–27. [CrossRef]
41. Qiao, Z.; Lu, Y.; He, T.; Wu, F.; Xu, X.; Liu, L.; Wang, F.; Sun, Z.; Han, D. Spatial expansion paths of urban heat islands in Chinese cities: Analysis from a dynamic topological perspective for the improvement of climate resilience. *Resour. Conserv. Recycl.* **2023**, *188*, 106680. [CrossRef]
42. Patz, J.A.; Campbell-Lendrum, D.; Holloway, T.; Foley, J.A. Impact of regional climate change on human health. *Nature* **2005**, *438*, 310–317. [CrossRef]
43. Yardley, J.; Sigal, R.J.; Kenny, G.P. Heat health planning: The importance of social and community factors. *Glob. Environ. Chang.* **2011**, *21*, 670–679. [CrossRef]

44. Manoli, G.; Fatichi, S.; Schläpfer, M.; Yu, K.; Crowther, T.W.; Meili, N.; Burlando, P.; Katul, G.G.; Bou-Zeid, E. Magnitude of urban heat islands largely explained by climate and population. *Nature* **2019**, *573*, 55–60. [CrossRef]
45. Anderson, G.B.; Bell, M.L. Heat waves in the United States: Mortality risk during heat waves and effect modification by heat wave characteristics in 43 US communities. *Environ. Health Perspect.* **2011**, *119*, 210–218. [CrossRef]
46. Li, D.; Bou-Zeid, E. Synergistic interactions between urban heat islands and heat waves: The impact in cities is larger than the sum of its parts. *J. Appl. Meteorol. Clim.* **2013**, *52*, 2051–2064. [CrossRef]
47. Grimm, N.B.; Faeth, S.H.; Golubiewski, N.E.; Redman, C.L.; Wu, J.; Bai, X.; Briggs, J.M. Global change and the ecology of cities. *Science* **2008**, *319*, 756. [CrossRef]
48. Liu, H.; Huang, B.; Yang, C. Assessing the coordination between economic growth and urban climate change in China from 2000 to 2015. *Sci. Total Environ.* **2020**, *732*, 139283. [CrossRef] [PubMed]
49. Monteiro, F.F.; Gonalves, W.A.; Melo, L.D.; Villavicencio, L.M.M.; Cássia, M. Assessment of urban heat islands in brazil based on modis remote sensing data. *Urban Clim.* **2021**, *35*, 100726. [CrossRef]
50. Shirani-Bidabadi, N.; Nasrabadi, T.; Faryadi, S.; Larijani, A.; Shadman Roudposhti, M. Evaluating the spatial distribution and the intensity of urban heat island using remote sensing, case study of isfahan city in iran. *Sustain. Cities Soc.* **2019**, *45*, 686–692. [CrossRef]
51. Zhang, M.D.; Feng, X.Q. Comprehensive evaluation of urban resilience in China. *Urban Issues* **2018**, *279*, 27–36.
52. Zhang, P.; Yu, W.; Zhang, Y.W. Spatial and temporal divergence of urban resilience in Shandong Province and its influencing factors. *Urban Issues* **2018**, *278*, 27–34.
53. Liu, L.; Lei, Y.; Zhuang, M.; Ding, S. The impact of climate change on urban resilience in the Beijing-Tianjin-Hebei region. *Sci. Total Environ.* **2022**, *827*, 154157. [CrossRef] [PubMed]
54. Duan, W.Q.; Joseph, D.M.; Adnan, K.; Ma, D. Industrial structure conditions economic resilience. *Technol. Forecast. Soc. Change* **2022**, *183*, 121944. [CrossRef]
55. Yang, C.; Liu, H.; Li, Q.; Cui, A.; Xia, R.; Shi, T.; Zhang, J.; Gao, W.; Zhou, X. Rapid Urbanization Induced Extensive Forest Loss to Urban Land in the Guangdong-Hong Kong-Macao Greater Bay Area, China. *Ecol. Indic.* **2021**, *115*, 106373. [CrossRef]
56. Chu, X.J. *Research on the Influence of Winter Climate Factors on the Snail Situation in Poyang Lake*; Chinese Center for Disease Control and Prevention: Beijing, China, 2010. (In Chinese)
57. Song, C.; Yang, J.; Wu, F.; Xiao, X.; Xia, J.; Li, X. Response characteristics and influencing factors of carbon emissions and land surface temperature in Guangdong Province, China. *Urban Clim.* **2022**, *46*, 101330. [CrossRef]
58. Wang, H.; Xue, H.; He, W.; Han, Q.; Xu, T.; Gao, X.; Liu, S.; Jiang, R.; Huang, M. Spatial-temporal evolution mechanism and dynamic simulation of the urban resilience system of the Guangdong-Hong Kong-Macao Greater Bay Area in China. *Environ. Impact Assess. Rev.* **2023**, *104*, 107333. [CrossRef]
59. Liu, L.; Lei, Y.; Fath, B.D.; Hubacek, K.; Yao, H.; Liu, W. The spatio-temporal dynamics of urban resilience in China's capital cities. *J. Clean. Prod.* **2022**, *379*, 134400. [CrossRef]
60. Chen, X.L.; Yu, L.X.; Lin, W.D.; Yang, F.Q.; Li, Y.P.; Tao, J.; Cheng, S. Urban resilience assessment from the multidimensional perspective using dynamic Bayesian network: A Case Study of Fujian Province, China. *Reliab. Eng. Syst. Saf.* **2023**, *238*, 109469. [CrossRef]
61. Han, S.; Wang, B.; Ao, Y.B.; Homa, B.; Chai, B.B. The coupling and coordination degree of urban resilience system: A case study of the Chengdu-Chongqing urban agglomeration. *Environ. Impact Assess. Rev.* **2023**, *101*, 107145. [CrossRef]
62. Shi, C.; Guo, N.; Gao, X.; Wu, F. How carbon emission reduction is going to affect urban resilience. *J. Clean. Prod.* **2022**, *372*, 133737. [CrossRef]
63. Liu, L.N.; Zhang, Z.C.; Ding, S.H.; Yang, F.; Fu, T.R. Combined effects of climate change on urban resilience in the Tibetan Plateau. *Environ. Impact Assess. Rev.* **2023**, *102*, 107186. [CrossRef]
64. Zhao, R.; Fang, C.; Liu, H.; Liu, X. Evaluating urban ecosystem resilience using the DPSIR framework and the ENA model: A case study of 35 cities in China. *Sustain. Cities Soc.* **2021**, *72*, 102997. [CrossRef]
65. Tang, D.C.; Li, J.N.; Zhao, Z.Q.; Valentina, B.; David, D.L. The influence of industrial structure transformation on urban resilience based on 110 prefecture-level cities in the Yangtze River. *Sustain. Cities Soc.* **2023**, *96*, 104621. [CrossRef]
66. Hu, X.; Su, Y.; Kefeng, R.; Song, F.; Xue, R. Measurement and influencing factors of urban traffic ecological resilience in developing countries: A case study of 31 Chinese cities. *Reg. Sustain.* **2021**, *2*, 211–223. [CrossRef]
67. Wang, H.; Liu, Z.; Zhou, Y. Assessing urban resilience in China from the perspective of socioeconomic and ecological sustainability. *Environ. Impact Assess. Rev.* **2023**, *102*, 107163. [CrossRef]
68. Jiao, L.D.; Wang, L.W.; Lu, H.; Fan, Y.W.; Zhang, Y.; Wu, Y. An assessment model for urban resilience based on the pressure-state-response framework and BP-GA neural network. *Urban Clim.* **2023**, *49*, 101543. [CrossRef]
69. Hwang, C.L.; Yoon, K.P. *Multiple Attribute Decision Making: Methods and Applications. A State-of-the-Art Survey*; Springer: Berlin/Heidelberg, Germany, 1981.
70. Hsu, P.F.; Hsu, M.G. Optimizing the information outsourcing practices of primary care medical organizations using entropy and TOPSIS. *Qual. Quant.* **2008**, *42*, 181–201. [CrossRef]
71. Jozi, S.A.; Shafiee, M.; MoradiMajd, N.; Saffarian, S. An integrated Shannon's Entropy–TOPSIS methodology for environmental risk assessment of Helleh protected area in Iran. *Environ. Monit. Assess.* **2012**, *184*, 6913–6922. [CrossRef]

72. Kingir, S.; Karakas, A.; Öztel, A. Evaluation of university employees' work behaviours performance via entropy based TOPSIS methods. *Elektron. Sos. Bilim. Derg.* **2016**, *15*, 1046–1058. [CrossRef]
73. Zhu, Y.; Zhang, C.; Fang, J.M.; Miao, Y.J. Paths and strategies for a resilient megacity based on the water-energy-food nexus. *Sustain. Cities Soc.* **2022**, *82*, 103892. [CrossRef]
74. Li, X.; Meng, X.; Ji, X.; Zhou, J.; Pan, C.; Gao, N. Zoning technology for the management of ecological and clean small-watersheds via k-means clustering and entropy-weighted TOPSIS: A case study in Beijing. *J. Clean. Prod.* **2023**, *397*, 136449. [CrossRef]
75. Wang, H.; Du, S.; Zhong, Y.; Liu, S.; Xu, T.; Zhao, Y.; He, W.; Xue, H.; He, Y.; Gao, X.; et al. Unveiling the impact mechanism of urban resilience on carbon dioxide emissions of the Pearl River Delta urban agglomeration in China. *Environ. Impact Assess. Rev.* **2024**, *105*, 107422. [CrossRef]
76. Wang, S.J.; Cui, Z.T.; Lin, J.J.; Xie, J.Y.; Su, K. The coupling relationship between urbanization and ecological resilience in the Pearl River Delta. *J. Geogr. Sci.* **2022**, *32*, 44–64. [CrossRef]
77. Song, Q.J.; Zhou, N.; Liu, T.L.; Siehr, S.A.; Qi, Y. Investigation of a "coupling model" of coordination between low-carbon development and urbanization in China. *Energy Policy* **2018**, *121*, 346–354. [CrossRef]
78. Hong, T.; Wang, B.; Li, L.L. The coupling relationship between urban resilience level and urbanization level in Hefei. *Math. Probl. Eng.* **2022**, *2022*, 7339005. [CrossRef]
79. Luo, X.; Cheng, C.; Pan, Y.; Yang, T.T. Coupling coordination and influencing factors of land development intensity and urban resilience of the Yangtze River Delta urban agglomeration. *Water* **2022**, *14*, 1083. [CrossRef]
80. Li, Y.F.; Li, Y.; Zhou, Y.; Shi, Y.L.; Zhu, X.D. Investigation of a coupling model of coordination between urbanization and the environment. *J. Environ. Manag.* **2012**, *98*, 127–133. [CrossRef] [PubMed]
81. Tomal, M. Evaluation of coupling coordination degree and convergence behaviour of local development: A spatiotemporal analysis of all polish municipalities over the period 2003–2019. *Sustain. Cities Soc.* **2021**, *71*, 102992. [CrossRef]
82. Tian, Y.; Huang, P.; Zhao, X. Spatial analysis, coupling coordination, and efficiency evaluation of green innovation: A case study of the Yangtze River Economic Belt. *PLoS ONE* **2020**, *15*, e0243459. [CrossRef] [PubMed]
83. Liu, N.; Liu, C.; Xia, Y.; Da, B. Examining the coordination between urbanization and eco-environment using coupling and spatial analyses: A case study in China. *Ecol. Indic.* **2018**, *93*, 1163–1175. [CrossRef]
84. Gencer. How to Make Cities More Resilient: A Handbook for Local Government Leaders. United Nations Office for Disaster Risk Reduction Making Cities Resilient 2030 (MCR2030). 2017. Available online: https://www.undrr.org/publication/how-make-cities-more-resilient-handbook-local-government-leaders-2017 (accessed on 10 March 2022).
85. Mahmood, R.; Pielke, R.A., Sr.; Hubbard, K.G.; Niyogi, D.; Dirmeyer, P.A.; McAlpine, C.; Bonan, G. Land cover changes and their biogeophysical effects on climate. *Int. J. Clim.* **2014**, *34*, 929–953. [CrossRef]
86. Li, X.; Zhou, Y.; Asrar, G.R.; Imhoff, M.; Li, X. The surface urban heat island response to urban expansion: A panel analysis for the conterminous United States. *Sci. Total Environ.* **2017**, *605*, 426–435. [CrossRef]
87. Song, Q.; Zhong, S.; Chen, J.; Yang, C.; Zhu, Y. Spatio-temporal evolution of city resilience in the Yangtze River Delta, China, from the perspective of statistics. *Sustainability* **2023**, *15*, 1538. [CrossRef]
88. Xi, Z.J.; Li, C.S.; Zhou, L.; Yang, H.J.; Burghardt, R. Built environment influences on urban climate resilience: Evidence from extreme heat events in Macau. *Sci. Total Environ.* **2023**, *859*, 160270. [CrossRef] [PubMed]
89. Nuruzzaman, M. Urban heat island: Causes, effects and mitigation measures-a review. *Int. J. Environ. Monit. Anal.* **2015**, *3*, 67–73. [CrossRef]
90. Giridharan, R.; Ganesan, S.; Lau, S.S.Y. Daytime urban heat island effect in high-rise and high-density residential developments in Hong Kong. *Energy Build.* **2004**, *36*, 525–534. [CrossRef]
91. Tran, D.X.; Pla, F.; Latorre-Carmona, P.; Myint, S.W.; Caetano, M.; Kieu, H.V. Characterizing the relationship between land use land cover change and land surface temperature. *ISPRS J. Photogramm. Remote Sens.* **2017**, *124*, 119–132. [CrossRef]
92. Chun, B.; Guldmann, J.M. Spatial statistical analysis and simulation of the urban heat island in high-density central cities. *Landsc. Urban Plan.* **2014**, *125*, 76–88. [CrossRef]

Disclaimer/Publisher's Note: The statements, opinions and data contained in all publications are solely those of the individual author(s) and contributor(s) and not of MDPI and/or the editor(s). MDPI and/or the editor(s) disclaim responsibility for any injury to people or property resulting from any ideas, methods, instructions or products referred to in the content.